Memoirs of the Faculty of Engineering, Nagoya University
Vol. 36, No. 1 (1984)

STUDY ON ROTATING CONDENSER WITH A SCRAPER

RYOTARO IZUMI, HAYATO MAEDA*
and HIROSHI YAMASHITA

Department of Mechanical Engineering

(Received May 1, 1984)

Abstract

A rotating condenser with a scraper is considered as a new method used to augment condensation heat transfer. We analyze the case where the condensate film on the vertical and the horizontal rotating cylinder is scraped off mechanically by the plate. In the vertical cylinder, the analytical solution for transient film condensation on a vertical plate is obtained, and it is applied to the infinitesimal element on the outer surface of vertical cylinder. The mean Nusselt number is calculated by integration over the whole surface of cylinder. Also, in the horizontal cylinder, an ordinary differential equation for a condensate film thickness is derived with several incidental conditions, and is integrated by a numerical method. The condensate state is classified according to the combination of the conditions. The enhancement due to scraping is arranged in terms of the mean Nusselt number ratio, and the effects of rotation speed, temperature difference between vapor and condenser surface are examined. The effects of the unscraped film thickness and the position of scraper are examined at the vertical and the horizontal rotating cylinder, respectively. Lastly, we report the experimental results for the condensation of refrigerant R-11 corresponding to the above analysis. The distributions of cylinder surface temperature and the mean heat transfer coefficients are obtained. The effects of rotation speed and temperature difference between vapor and condenser surface are made clear. The enhancement due to scraping is arranged in terms of the mean Nusselt number ratio and compared with analytical results.

* Faculty of Science and Technology, Meijo University.

CONTENTS

Nomenclature

A : heat transfer surface area
A, B, C : functions
c_{PL} : specific heat at constant pressure
g : acceleration of gravity
Ga_l, Ga_d : Galilei number
Gr_l, Gr_R : Grashof number
H : ratio of sensible to latent heat
H' : modified ratio of sensible to latent heat
I, J : node-numbers in finite difference method
L, L' : latent heat, modified latent heat
l : cylinder height
$\dot{m}$: rate of condensation
N : rotation speed
Nu : Nusselt number
Nu_m : mean Nusselt number
P : pressure
Pr : Prandtl number
Q : quantity of heat or flow rate
R : radius of cylinder
Re_R : Reynolds number due to peripheral velocity
s : parameter
$T, \Delta T$: temperature, temperature difference
t : time
u, u_{sf} : velocity, peripheral velocity
V : volume
$\dot{V}$: flow rate per unit width
y : co-ordinate measuring radial distance outward from cylinder surface
z : co-ordinate measuring vertical distance along cylinder axis
z^* : the lowest position of steady state condensate film at time when the cylinder has rotated one turn
α : heat transfer coefficient
δ : condensate film thickness
λ : thermal conductivity
ν : kinematic viscosity
ρ : density
ϕ : angle from scraper position or cylinder top, or diameter

subscripts
eps : very small amount

f : falling position of condensate film
i : position of initial condition
in : initial value
L : liquid
l : position $z=l$ or cylinder length
m : mean
N : $N=N$ in rotation
R : cylinder radius as characteristic length
s : saturated vapor or non rotation without scraper
sc : position of scraper
sf : outer surface of cylinder
ss : steady state
t : $t=t$ in time or position of transition in liquid film
top : top of cylinder
v : vapor
w : haet transfer surface
z : position $z=z$
0 : unscraped film thickness
ϕ : position $\phi=\phi$
$'$: modification
$\wedge$: dimensionless presentation
$*$: dimensionless presentation

Chapter 1. Analysis of Condensation on Outer Surface of Vertical Cylinder

1. Introduction

Recently, the researches for enhancing the performance of the condensers have been promoted more and more widely and eagerly, because of the requirements in many fields including refrigerators, air conditioners and other various industrial equipments, larger scale power generating plants, effective use of thermal energy in small-temperature difference in view of energy conservation, and so forth[1,2]. Meanwhile, many methods for enhancing heat transfer have been proposed. Especially, the film condensation heat transfer is a practically important; various devices have been proposed to obtain thinner condensate film working as a heat transfer resistance element. These examples include the tube with a small-fin array[3] using surface tension, the same modified by attaching a circular disc to remove the condensate film[2], a device utilizing electric field to pull off the condensate film[4], another device attached with a porous plate using capillary action[5], etc.

The authors attempted a more direct and positive method to remove the condensate film on the heat transfer tube; a condenser was rotated around its axis and the condensate film was mechanically scraped off by a scraper closely attached on its outer surface. Regarding the rotary type condenser, there are many contributions so far including circular disc[6], cone[7], vertical[8] and horizontal[9] tubes, etc.; in these methods, the condensate film on the outer surface is separated by the centrifugal force in rotating field or circumferential shear force. However, substantially

these effects will not be exerted at lower rotation speed, therefore, it has been pointed out that the rotation speed should considerably be high. This is a practical problem in view of energy conservation and equipment integrity. The authors think that, by adding a scraper to this rotating condenser, effect of the heat transfer augmentation would largely be improved even at lower rotation speed. This type of rotary scraper heat transferring system has not yet been reported for the condenser, although there is a report for scraping-off the thermal boundary layer in the single phase flow[10].

Important items of the rotating condenser with a scraper include how to drive the rotary part and how to seal. However, the heat transfer tube itself may be smooth surface and, by means of the scraper, vapor side is in turbulence, so that noncondensable gas will not be deposited near the heat transfer surface. These are the merits of this system. In principle, moreover, its efficiency would greatly be enhanced by using many scrapers and making rotation speed larger. Therefore, this system will be hopeful in effect.

In this chapter as the lst report of this rotating condenser with a scraper, an analysis of condensation on the outer surface of vertical cylinder is described. Based on an analytical solution by Sparrow et al. for transient laminar film condensation on a vertical plate[11], the mean Nusselt number is obtained over the entire surface of a cylinder, thereby the enhancement due to scraping is calculated. Especially corresponding to the experiment shown in Chapter 3, refrigerant R-11 is employed to study the effect of unscraped film thickness as a practical problem. Then, the refrigerant is compared with other kinds of refrigerant.

2. Theoretical Analysis

In this analysis, an arrangement is assumed as shown in Fig. 1. 1 there is an acceleration of gravity g, then a vertical cylinder of radius R is placed in saturated vapor and rotated around its own axis. Then, the condensate on the outer surface cooled to a constant temperature is attempted to scrape off using a plate installed in close contact with the cylinder axis or slightly separated therefrom. In addition, the assumption for the analysis includes that rotation speed N be small enough, the centrifugal force acting on the condensate film be negligible, and the condensate would not be splashed without creating any relative motion for the circumferential direction of the outer surface of the cylinder. At that time, let's assume an infinitesimal element $lRd\phi$ on the cylinder surface and also assume that the liquid film is scraped off at time $t=0$ and, after one revolution, it is again scraped off at $t=1/N$. Then, we can assume that, in between times $t=0$ and

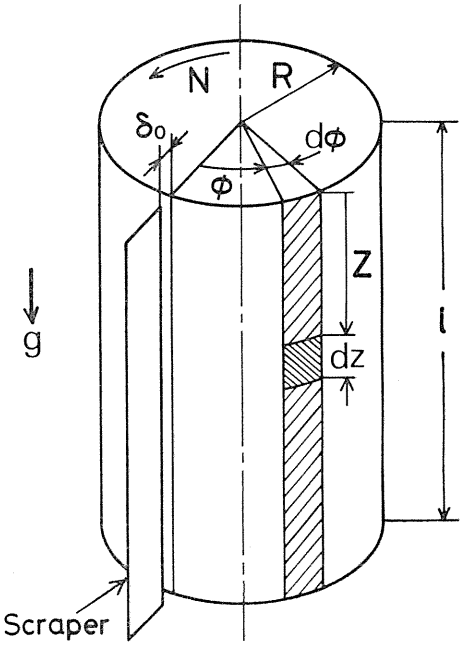

Fig. 1. 1 Analytical model.

$t=1/N$ and at an angle ϕ from the scraper, a condition of $t=\phi/2\pi N$ in the transient laminar film condensation on a vertical plate is realized. Consequently, first we should deal with the transient laminar film condensation on a vertical plate and then, by using the result, we would proceed with studying the condensation conditions on a total surface of the cylinder.

2. 1. Transient condensation on vertical plate

The analysis of Sparrow, et al.[11] is extended for the case of finite initial thickness of condensate film. Then, using the method of characteristic curve, the solution is calculated.

2. 1. 1. Fundamental equations

In dealing with condensate film, the influence from inertia force and vapor friction on the interface between vapor and liquid are neglected. Also, temperature distribution is assumed linear. Then, velocity u and temperature T are expressed as follows:

$$u=\frac{\rho_L-\rho_V}{2\rho_L\nu_L}g\delta^2\left[2\frac{y}{\delta}-\left(\frac{y}{\delta}\right)^2\right] \tag{1}$$

$$T=T_s+(T_s-T_w)\left(\frac{y}{\delta}-1\right) \tag{2}$$

where y and δ are the radial distance outward from the cylinder surface and the condensate film thickness, respectively. Also, T_s and T_w are temperatures of saturated vapor and the cylinder wall surface, respectively. On the other side, the transient energy balance of infinitesimal element at position $z=z$ of liquid film can be represented as follows:

$$\rho_L L\left[\frac{\partial}{\partial z}\left(\int_0^\delta u\,dy\right)+\frac{\partial\delta}{\partial t}\right]-\rho_L c_{PL}\left[\frac{\partial}{\partial z}\left\{\int_0^\delta u(T-T_s)dy\right\}+\frac{\partial}{\partial t}\left\{\int_0^\delta (T-T_s)dy\right\}\right]=\lambda_L\left(\frac{\partial T}{\partial y}\right)_{y=0} \tag{3}$$

In addition, the initial condition for the condensate film thickness is assumed by the following equation in consideration of a case with rotary scraping,

$$t=0:\ \delta=\begin{cases}\delta_{ss}(z) & (0\leqq z\leqq z_0)\\ \delta_0 & (z_0\leqq z\leqq l)\end{cases} \tag{4}$$

where $\delta_{ss}(z)$ is the stationary condensate film thickness, δ_0 is the thickness of unscraped film, and z_0 is a value of z with which $\delta_{ss}(z)=\delta_0$ holds valid. On the other hand, the boundary condition becomes as follows:

$$z=0:\ \delta=0 \tag{5}$$

Substituting Eqs. (1) and (2) into Eq. (3) and eliminating dimensions, the following equation is obtained.

$$4\hat{\delta}^3\frac{\partial\hat{\delta}}{\partial\hat{z}}+2\hat{\delta}\frac{\partial\hat{\delta}}{\partial\hat{t}}=1 \qquad (3)'$$

In the equation above, the following conversion is employed for dimensionless presentation.

$$\hat{z}\equiv\frac{z}{l},\quad \hat{t}\equiv\frac{t}{t'_{lss}},\quad \hat{\delta}\equiv\frac{\delta}{\delta_{lss}}$$

In the above, t'_{lss} and δ_{lss} used for dimensionless presentation are defined by the following equations. Their physical significance will later be described.

$$t'_{lss}\equiv t_{lss}/\{1-\hat{z}_0^{\frac{1}{2}}\},$$

$$N\cdot t_{lss}\equiv\left(\frac{Pr}{Gr_lH'}\right)^{\frac{1}{2}}\frac{Nl^2}{\nu_L}\left(1+\frac{1}{8}H'\right)\left\{1-\hat{z}_0^{\frac{1}{2}}\right\},$$

$$\frac{\delta_{lss}}{l}\equiv\left(\frac{4H'}{Gr_lPr}\right)^{\frac{1}{4}}$$

The dimensionless numbers used in the above are defined by the following equations.

$$Gr_l\equiv\frac{l^3g(\rho_l-\rho_v)}{\rho_L\nu_L^2},$$

$$Pr\equiv\frac{c_{PL}\rho_L\nu_L}{\lambda_L},$$

$$H'\equiv\frac{c_{PL}(T_s-T_w)}{L'},\quad \left\{L'\equiv L+\frac{3c_{PL}(T_s-T_w)}{8}\right\}$$

As will be explained later, $\delta_{ss}(z)$ and z_0 are calculated by the following equations.

$$\frac{\delta_{ss}(z)}{\delta_{lss}}=\left(\frac{z}{l}\right)^{\frac{1}{4}},\quad \frac{\delta_0}{\delta_{lss}}=\left(\frac{z_0}{l}\right)^{\frac{1}{4}}$$

2. 1. 2. Analysis by the method of characteristic curve

Partial differential equation (3)′ has a solution $\hat{\delta}=\hat{\delta}(\hat{z},\hat{t})$ which is the same as the snlution of the following simultaneous differential equations expressed by parameter s[12].

$$\frac{d\hat{z}}{ds}=4\hat{\delta}^3,\quad \frac{d\hat{t}}{ds}=2\hat{\delta},\quad \frac{d\hat{\delta}}{ds}=1 \qquad (6)$$

The solution of the equation above is given by the following equations, where $\hat{z}_{in}$, $\hat{t}_{in}$, and $\hat{\delta}_{in}$ are initial values of $\hat{z}$, $\hat{t}$, and $\hat{\delta}$ at $s=0$.

$$\left.\begin{aligned}\hat{z}&=(s+\hat{\delta}_{in})^4+\hat{z}_{in}-\hat{\delta}_{in}^4\\ \hat{t}&=(s+\hat{\delta}_{in})^2+\hat{t}_{in}-\hat{\delta}_{in}^2\\ \hat{\delta}&=s+\hat{\delta}_{in}\end{aligned}\right\} \qquad (7)$$

By eliminating s, the following equations of characteristic curve are obtained.

$$\begin{aligned}&[(\hat{z}-\hat{z}_{in})+\hat{\delta}_{in}{}^4]^{\frac{1}{4}}\\&=[(\hat{t}-\hat{t}_{in})+\hat{\delta}_{in}{}^2]^{\frac{1}{2}}=\hat{\delta}\end{aligned}\tag{8}$$

When Eq. (4) for initial conditions and Eq. (5) for boundary conditions are described in the following 3 cases, indicating the same forms as in the above.

$s=0$:

$$\left.\begin{array}{lllll}\text{(i)} & \hat{z}_{in}=\hat{z}_{in}(0\leqq\hat{z}_{in}\leqq\hat{z}_0), & \hat{t}_{in}=0, & \hat{\delta}_{in}=\hat{\delta}_{ss}(\hat{z}_{in})\\ \text{(ii)} & \hat{z}_{in}=\hat{z}_{in}(\hat{z}_0\leqq\hat{z}_{in}\leqq 1), & \hat{t}_{in}=0, & \hat{\delta}_{in}=\hat{\delta}_0\\ \text{(iii)} & \hat{z}_{in}=0, & \hat{t}_{in}=\hat{t}_{in}, & \hat{\delta}_{in}=0\end{array}\right\}\tag{9}$$

In this case, the characteristic curve equation becomes as follows:

$$\left.\begin{array}{lll}\text{(i)} & [(\hat{z}-\hat{z}_{in})+\hat{\delta}_{ss}{}^4(\hat{z}_{in})]^{\frac{1}{4}}=[\hat{t}+\hat{\delta}_{ss}{}^2(\hat{z}_{in})]^{\frac{1}{2}}=\hat{\delta}\\ \text{or,} & & \\ & [\hat{z}]^{\frac{1}{4}}=[\hat{t}+\hat{z}_{in}{}^{\frac{1}{2}}]^{\frac{1}{2}} & =\hat{\delta}\\ \text{(ii)} & [(\hat{z}-\hat{z}_{in})+\hat{\delta}_0^4]^{\frac{1}{4}}=[\hat{t}+\hat{\delta}_0^2]^{\frac{1}{2}} & =\hat{\delta}\\ \text{or,} & & \\ & [(\hat{z}-\hat{z}_{in})+\hat{z}_0]^{\frac{1}{4}}=[\hat{t}+\hat{z}_0{}^{\frac{1}{2}}]^{\frac{1}{2}} & =\hat{\delta}\\ \text{(iii)} & [\hat{z}]^{\frac{1}{4}}=[\hat{t}-\hat{t}_{in}]^{\frac{1}{2}} & =\hat{\delta}\end{array}\right\}\tag{10}$$

The relationship between $\hat{z}$ and $\hat{\delta}$ in (i) and (iii) does not contain parameter $\hat{z}_{in}$ or $\hat{t}_{in}$, therefore, independent of $\hat{t}$. That is, this gives the solution corresponding to the steady state. On the other hand, relationship (ii) between $\hat{t}$ and $\hat{\delta}$ gives the solution for unsteady state; no parameter is contained while independent of $\hat{z}$. The limiting characteristic curve between (i) or (iii) and (ii) sectionalizes the regions of steady and unsteady states; putting $\hat{z}_{in}=\hat{z}_0$ in (i) or (ii), the time to achieve steady state $\hat{t}_{ss}$ becomes as follows:

$$\hat{t}_{ss}=\hat{z}^{\frac{1}{2}}-\hat{z}_0{}^{\frac{1}{2}}\tag{11}$$

Eventually, condensate film thickness $\hat{\delta}$ is given by the following equations for steady and unsteady states.

$$\left.\begin{array}{ll}\hat{\delta}=[\hat{t}+\hat{z}_0{}^{\frac{1}{2}}]^{\frac{1}{2}} & (\hat{t}\leqq\hat{t}_{ss})\\ \hat{\delta}_{ss}=\hat{z}^{\frac{1}{4}} & (\hat{t}\geqq\hat{t}_{ss})\end{array}\right\}\tag{12}$$

Especially, when $z=l$, $\hat{t}_{ss}=1-\hat{z}_0{}^{\frac{1}{2}}$ holds. In other words, $t_{ss}/t_{lss}=1$, and $\hat{\delta}_{ss}=1$, namely $\delta_{ss}/\delta_{lss}=1$. In consequence, it is understood that t_{lss} and δ_{lss} represent the

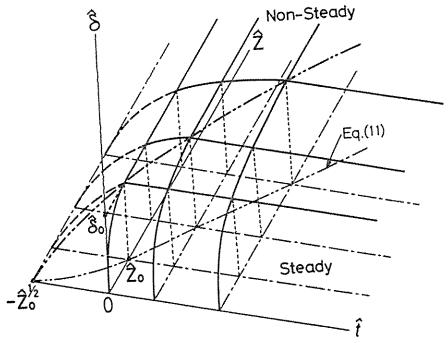

Fig. 1. 2 Schematic diagram of characteristic curve method.

time to achieve steady state and the stationary film thickness at the lowest end of the cylinder, i. e. $z=l$.

The integral hypersurface obtained above is schematically shown in Fig. 1. 2. The bold solid lines show the characteristic curves on this surface, as described with fixed $\hat{z}$ or $\hat{t}$. Also, the bold chain lines show the limiting characteristic curve between (i) and (ii), and the small chain lines show a projection on plane $\hat{z}-\hat{t}$, i. e. Eq. (11). The line of intersection between surface $\hat{z}-\hat{\delta}$ and the integral hypersurface corresponds to Eq. (4), i. e. the equation of initial conditions. The broken lines show the integral hypersurface extended in $\hat{t}<0$.

2. 1. 3. Local Nusselt number

The local heat transfer coefficient α_{zt} and the local Nusselt number Nu_{zt} are defined by the following equations.

$$\alpha_{zt}\equiv\frac{\lambda_L}{\delta},\quad Nu_{zt}\equiv\frac{\alpha_{zt}\cdot l}{\lambda_L}=\frac{l}{\delta} \tag{13}$$

By substituting Eq. (12), the following equations are obtained.

$$Nu=\begin{cases} Nu_{zt}=[\hat{t}+\hat{z}_0^{\frac{1}{2}}]^{-\frac{1}{2}}\dfrac{l}{\delta_{lss}} \\ Nu_{zss}=[\hat{z}]^{-\frac{1}{4}}\dfrac{l}{\delta_{lss}} \end{cases} \tag{14}$$

2. 2. Condensation on the outer surface of vertical cylinder

The analysis in the previous paragraph provides the local Nusselt number in $z=0\sim l$ at an arbitrary time. Using this data, the mean Nusselt number can be obtained on the entire outer surface of cylinder. At that time, an unsteady state of the time $t=\phi/2\pi N$ would be realized in $z=0\sim l$ on the position $\phi=\phi$. In addition, one turn of the cylindrical surface corresponds to $\phi=0\sim 2\pi$. Therefore, mean Nusselt number $(Nu_m)_N$ is given by the following equation.

$$\begin{aligned}(Nu_m)_N&\equiv\frac{1}{l2\pi R}\int_0^l\int_0^{2\pi}NuRd\phi dz\\&=\frac{N}{l}\int_0^l\int_0^{\frac{1}{N}}Nu\,dtdz\\&=N\cdot t'_{lss}\int_0^1\int_0^{\frac{1}{Nt'_{lss}}}Nu\,d\hat{t}d\hat{z}\end{aligned} \tag{15}$$

Especially with no rotation, i. e. $N=0$ and $\hat{z}_0\geqq 1$, the following equation is obtained by substituting Nu_{zss} of Eq. (14) into Eq. (15).

$$(Nu_m)_{N=0}=\int_0^1 Nu_{zss}d\hat{z}=\frac{4}{3}\frac{l}{\delta_{lss}} \tag{16}$$

Generally with $N=N$, the condensate film is separated to steady state and unsteady state portions. Assuming the lowest position z^* where the condensate film is in steady state at time $t=1/N$ when the cylinder has rotated one turn, the following equation is obtained from Eq. (11).

$$\frac{1-\hat{z}_0^{\frac{1}{2}}}{N\cdot t_{lss}}=\hat{z}^{*\frac{1}{2}}-\hat{z}_0^{\frac{1}{2}}$$

Especially when $z^*=l$, $Nt_{lss}=1$ holds. By substituting Eq. (14) into Eq. (15), the following equation is obtained for $\hat{z}^*\leqq 1$ i. e. $Nt_{lss}\geqq 1$.

$$\begin{aligned}(Nu_m)_N=Nt'_{lss}\Bigg[&\int_0^{\hat{z}_0}\int_0^{\frac{1}{Nt'_{lss}}}Nu_{zss}d\hat{t}d\hat{z}\\&+\int_{\hat{z}_0}^{\hat{z}^*}\left\{\int_0^{\frac{t_{ss}}{t'_{lss}}}Nu_{zt}d\hat{t}+\int_{\frac{t_{ss}}{t'_{lss}}}^{\frac{1}{Nt'_{lss}}}Nu_{zss}d\hat{t}\right\}d\hat{z}\\&+\int_{\hat{z}^*}^1\int_0^{\frac{1}{Nt'_{lss}}}Nu_{zt}d\hat{t}d\hat{z}\Bigg]\end{aligned} \tag{17}$$

On the other hand, for $\hat{z}^*\geqq 1$ i. e. $Nt_{lss}\leqq 1$, Eq. (18) is obtained.

$$\begin{aligned}(Nu_m)_N=Nt'_{lss}\Bigg[&\int_0^{\hat{z}_0}\int_0^{\frac{1}{Nt'_{lss}}}Nu_{zss}d\hat{t}d\hat{z}\\&+\int_{\hat{z}_0}^1\left\{\int_0^{\frac{t_{ss}}{t'_{lss}}}Nu_{zt}d\hat{t}+\int_{\frac{t_{ss}}{t'_{lss}}}^{\frac{1}{Nt'_{lss}}}Nu_{zss}d\hat{t}\right\}d\hat{z}\Bigg]\end{aligned} \tag{18}$$

By integrating Eqs. (17) and (18) and arranging with the mean Nusselt number ratio to the case of non-rotation, i. e. $(Nu_m)_N/(Nu_m)_{N=0}$, the following equation is obtained,

$$\frac{(Nu_m)_N}{(Nu_m)_{N=0}}\begin{cases}=C^{\frac{3}{2}}+\dfrac{3}{2}A\left\{\left(1-\dfrac{3}{5}C^2\right)C^{\frac{1}{2}}+\dfrac{2}{3}C^{\frac{3}{2}}B^2-\dfrac{1}{15}B^5-B\right\}\\ \qquad\qquad\{\hat{z}^*\leqq 1(Nt_{lss}\geqq 1)\}\\ =1+\dfrac{3}{2}A\left\{\dfrac{2}{5}+\dfrac{2}{3}B^2-\dfrac{1}{15}B^5-B\right\}\\ \qquad\qquad\{\hat{z}^*\geqq 1(Nt_{lss}\leqq 1)\}\end{cases} \tag{19}$$

where $A=Nt'_{lss}$, $B\equiv\hat{z}_0^{\frac{1}{4}}=\hat{\delta}_0$ and $C\equiv A^{-1}+B^2$.

3. Analyzed Results and Discussions

Corresponding to the experiment in Chapter 3, an example of numerical calculations

with refrigerant R-11 is shown with constant values at characteristic temperatures. Physical properties are used 293.2 K and 303.2 K for liquid and vapor phases, respectively[13]. Also, the parameters used for presentation are temperature difference $\Delta T=T_s-T_w$(K) and rotation speed N (rpm) with constant values of the cylinder radius $R=0.0505$ m and height $l=0.705$ m.

3. 1. *Transient film condensation on a vertical plate*

Using Eqs. (11) and (12), condensate film thickness δ can be obtained for any t and z. The distribution of δ at $z=0\sim l$ is shown in Fig. 1. 3 with $\Delta T=10.0$ K and $\delta_0=0.03$ mm and a parameter of t. The curve and the straight line show the steady and the unsteady distributions, respectively. Each straight lines branches from a position of z corresponding to each t_{ss}. The relationship between condensate film thickness at $z=l$ and ΔT is shown in Fig. 1. 4 with $\delta_0=0.03$ mm and a parameter of t. The δ becomes smaller where ΔT decreases. In this case, the change due to t also becomes less. Figure 1.5 shows the relationship between the time to achieve steady state t_{lss} and ΔT with $\delta_0=0.0$, 0.03, and 0.05 mm. Here t_{lss} becomes larger with $\delta_0=0.0$ and 0.03 mm, when ΔT decreases. With $\delta_0=0.05$ mm, t_{lss} has a peak when ΔT changes. Moreover, t_{lss} is smaller with larger δ_0.

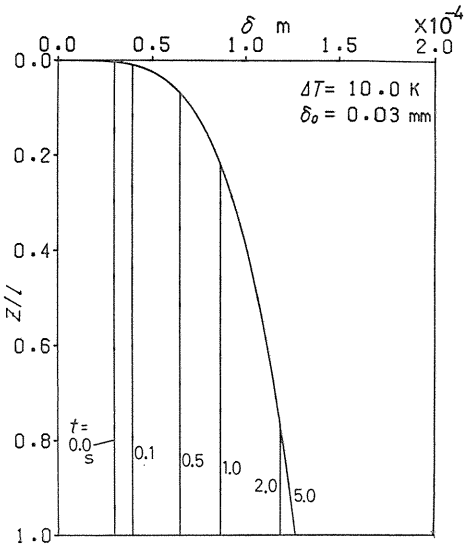

Fig. 1. 3 Distribution of condensate film thickness (Vertical plate, $\Delta T=10.0$K, $\delta_0=0.03$ mm).

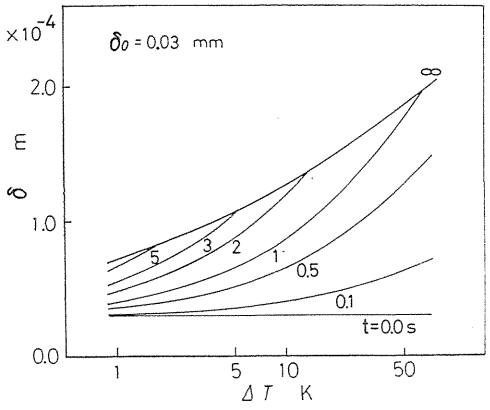

Fig. 1. 4 Relations between condensate film thickness and ΔT ($z=l$ $\delta_0=0.03$ mm).

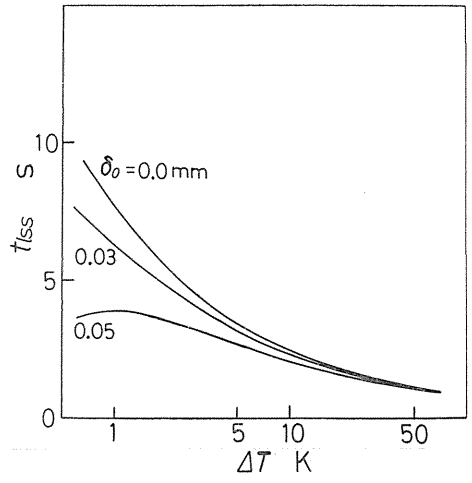

Fig. 1. 5 Relations between the time to achieve steady state and ΔT (R-11).

3. 2. Condensation on the outer surface of vertical cylinder

3. 2. 1. Distribution of condensate film thickness

Figure 1. 6 shows the distribution of condensate film thickness in the ϕ direction at the lowest end $z=l$ on the outer surface of the cylinder, with a parameter of N and $\Delta T=20.0$K and $\delta_0=0.0$ mm. The condensate film becomes thicker when ϕ increases; at $N=10$ rpm and 20 rpm, steady states occur on points A and B, respectively. With the values of ϕ larger than these, the condensate film remains constant. At $N=80$ rpm, the condensate is scraped off again before reaching a steady thickness.

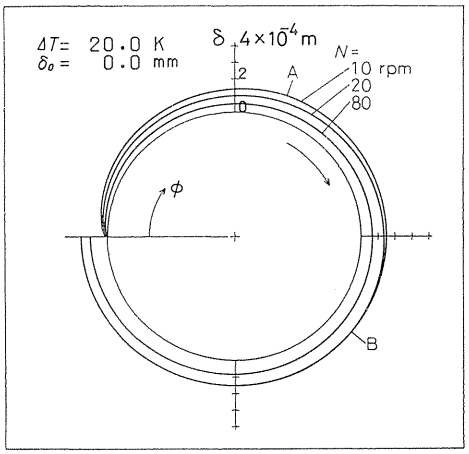

Fig. 1. 6 Distributions of condensate film thickness (On outer surface of cylinder, $\Delta T=20.0$K, $\delta_0=0.0$mm).

3. 2. 2. Mean Nusselt number

The relationship between the mean Nusselt number ratio $(Nu_m)_N/(Nu_m)_{N=0}$ and the product of the rotation speed and the time to achieve steady state Nt_{lss} is shown in Fig. 1. 7 with a parameter of dimensionless unscraped film thickness $\hat{\delta}_0$. $(Nu_m)_N/(Nu_m)_{N=0}$ becomes larger when Nt_{lss} is larger, i. e. the rotation speed is larger or the time to achieve steady state is longer. On the contrary, it becomes smaller when $\hat{\delta}_0$ is larger, and when $\hat{\delta}_0=1$, the ratio becomes 1. This figure has completely been made dimensionless, available for general purposes.

Figures 1. 8 (a), (b), and (c) show the influence of N, ΔT, and δ_0 on the mean Nusselt number ratio. The ratio is larger with larger N. In $\delta_0 \leqq 0.01$ mm, the ratio

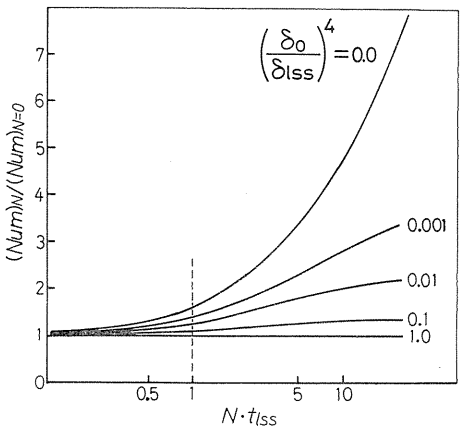

Fig. 1. 7 Relations between mean Nusselt number ratio and Nt_{lss}.

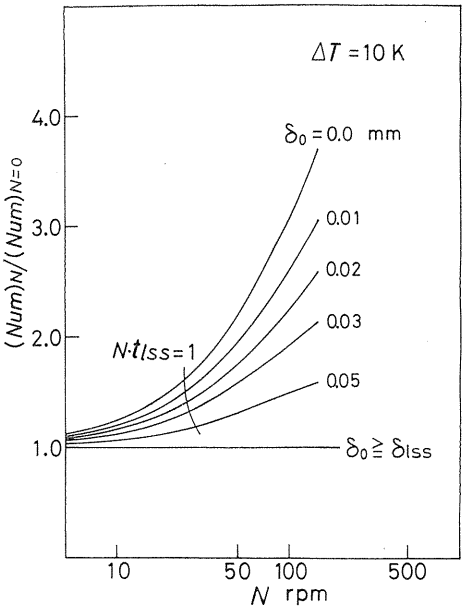

Fig. 1. 8 (a) Effects of N ($\Delta T=10.0$K)

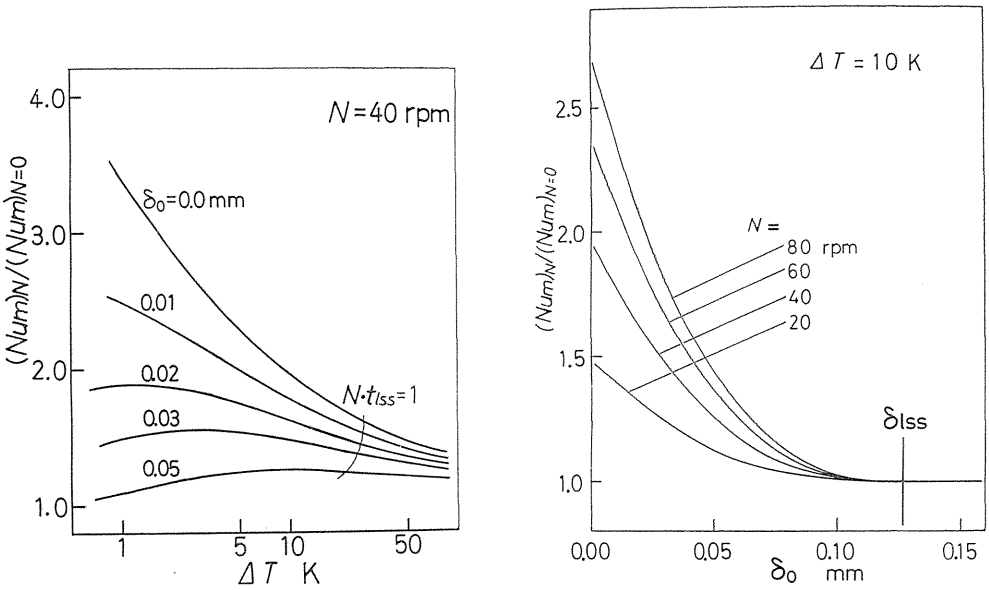

(b) Effects of ΔT (N=40 rpm) (c) Effects of δ_0 (ΔT=10.0 K)

Fig. 1. 8 Effects of N, ΔT, and δ_0 on mean Nusselt number ratio (R-11).

becomes larger when ΔT is smaller, and in $\delta_0 \geqq 0.02$ mm, the ratio has a peak value depending on ΔT. Also, the ratio decreases when δ_0 becomes larger and, where it approaches δ_{lss}, the ratio agrees with 1 regardless of N.

3. 2. 3. Comparison with various kinds of refrigerant

The influence of N and ΔT on the mean Nusselt number ratio is shown in Figs. 1. 9 (a) and (b) with refrigerant R-11, R-22 and water. Physical properties

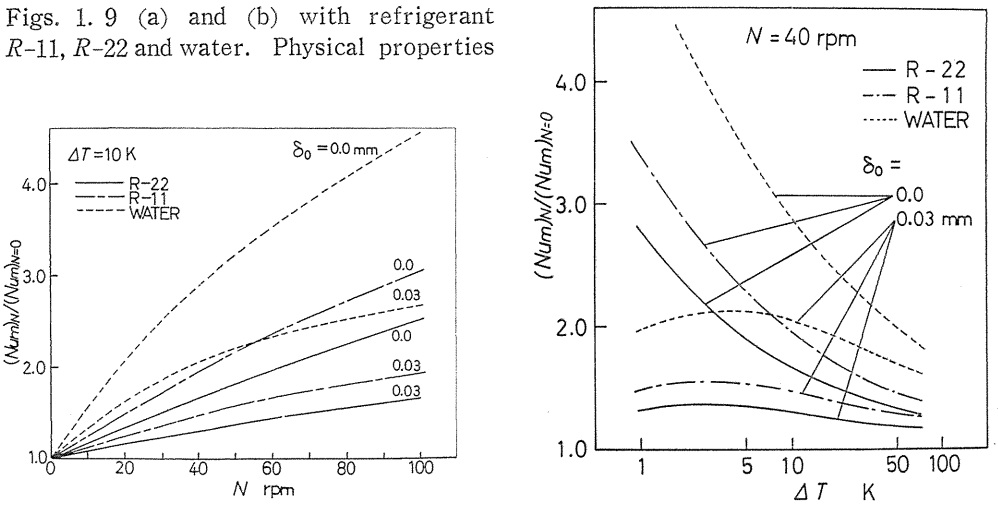

(a) Effects of N (ΔT=10.0 K) (b) Effects of ΔT (N=40 rpm)

Fig. 1. 9 Effects of N and ΔT on mean Nusselt number ratio (Various kinds of refrigerant).

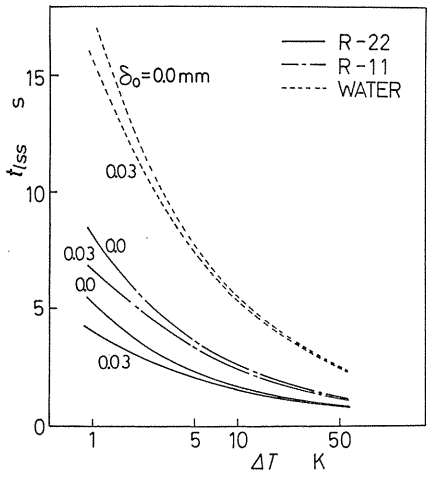

of R-22 and water are used values at the same temperature as R-11. The ratios are ranked, larger to smaller, for water, R-11 and R-22. Especially with water, the effect of scraping is significant. This is because, as shown in Fig. 1. 10, the time to achieve steady state for water is larger than those of the others.

Fig. 1. 10 Relations between the time to achieve steady state and ΔT (Various kinds of refrigerant).

4. Conclusions

A new method was proposed to augment heat transfer in condensation; a vertical cylinder was rotated and the condensate film was scraped off from the outer surface. According to a theoretical analysis, the following conclusions were obtained.

(1) A solution has been derived using the method of characteristic curve for the transient film condensation on a vertical plate. The method is applied to the condensation on the outer surface of a vertical cylinder to obtain the mean Nusselt number. Thereby, the effect of scraping can quantitatively be denoted in terms of the mean Nusselt number ratio.

(2) The mean Nusselt number ratio is a function of a product of the rotation speed and the time to achieve steady state i. e. Nt_{lss} and the dimensionless unscraped thickness $\hat{\delta}_0$. With the larger Nt_{lss} and smaller $\hat{\delta}_0$, the ratio becomes larger.

(3) Particularly with R-11, it was examined how the mean Nusselt number ratio would be affected by rotation speed N, the difference of temperatures between saturated vapor and heat transfer surface i. e. ΔT, and unscraped film thickness δ_0. As a result, it was revealed that this ratio became larger with the larger N and smaller ΔT and δ_0, and that where δ_0 becomes considerably large, the ratio has a maximum value relating to ΔT.

(4) Regarding a comparison between water, R-11 and R-22, the mean Nusselt number ratios are descending in that order. Especially with water, the effect of scraping is significant.

(Appendix) Analysis by the Finite Difference Method

In addition to the analysis using the characteristic curve method, the finite difference method was also used for another analysis. This is described as follows.

Node numbers are represented by I and J in terms of z and t. Also, the grid spacings of finite difference are expressed by Δz and Δt. Then, the condensate film thickness and its differential coefficients are expressed as follows:

$$\delta(z,\ t) \longrightarrow \delta^n(I+1,\ J+1)$$

$$\frac{\partial\delta}{\partial z} \longrightarrow \frac{\delta^{n+1}(I+1,\ J+1)-\delta^{n+1}(I,\ J+1)}{\Delta z}$$

$$\frac{\partial\delta}{\partial t} \longrightarrow \frac{\delta^{n+1}(I+1,\ J+1)-\delta^{n+1}(I+1,\ J)}{\Delta t}$$

where n denotes the number of steps in repeated calculations. By substituting these in Eq. (3)′, $\delta^{n+1}(I+1,\ J+1)$ is solved, then the calculation was repeated using the SOR method including the initial and boundary conditions. Attached Fig. 1 shows an example of the calculation for the timely change of condensate film thickness. The result with the finite difference method (FDM) is different from that with the characteristic curve method (CM); the solution of the former denotes a continuous, moderate slope in the connection between the steady and unsteady states. As far as the present analysis is concerned, the CM could provide a satisfactory solution. But if the initial condition or the boundary condition becomes complicated or physical properties change, the solution should be obtained using the FDM.

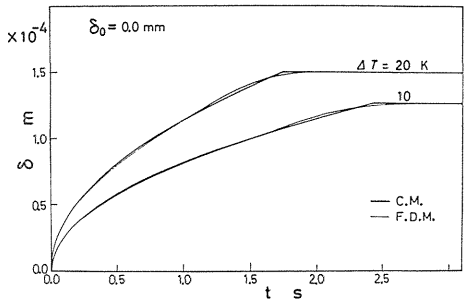

Attached Fig. 1 Variations of condensate film thickness ($z=l$, Finite difference method).

Chapter 2. Analysis of Condensation on Outer Surface of Horizontal Cylinder

1. Introduction

The authors have proposed in the previous chapter the rotating condenser with a scraper to augment heat transfer coefficient in condensation. In the previous chapter, described was the analysis of the condensation on the outer surface of a vertical cylinder together with the enhancement due to scraping. Subsequently in this chapter the analysis for a horizontal rotating cylinder is described; the cylinder is rotated around its axis and the condensate film is mechanically scraped off by a scraper closely attached on its outer surface.

There are many reports so far for the horizontal rotating condenser[9,14~16], in which it is pointed out that, at a low speed, condensate film tends to stagnate on the heat transfer tube while the heat transfer performance decreases. If the scraper is used for low speed rotation, the effect of scraping would be larger than with a vertical cylinder. Also, another technical problem is where to install the scraper, because circumferential velocity of the outer surface is affected by the gravity depending on angular position.

As described above, the horizontal cylinder has considerably different aspect from the vertical cylinder of the previous chapter. Therefore, the analysis for the horizontal cylinder requires a completely different method. Singer, et al.[9] have derived an ordinary differential equation for the case without scraper. The authors are proposing a modified method of the above by adding several incidental conditions, while also covering the case with a scraper in a universal manner. Using this proposed method, various condensate film conditions are theoretically classified and effect of scraping is quantitatively denoted in this chapter. In these processes of the analysis, data are presented for the distribution of condensate film thicknesses, the distribution of local heat transfer coefficient, and the mean Nusselt number. Especially, corresponding to the experiment shown in Chapter 3, refrigerant R-11 is employed to study the effects of rotation speed and the temperature difference between vapor and the condenser surface. Further, a comparative check is performed for the influence of installation position of the scraper.

2. Theoretical Analysis

An analytical model of Fig. 2. 1 is assumed for the analysis; a cylinder of radius R is horizontally positioned in saturated vapor and rotated around its axis under gravity acceleration g, then the condensate liquid on the outer surface cooled to a constant temperature is scraped off with a scraper attached parallel to the axis and in close contact with the cylinder surface. In addition, other assumptions are that rotation speed N is so small that the centrifugal force acting on the condensate film can be neglected and that the condensate liquid is not splashed away but drops at an angular position lower than the cylinder axis. Also, another assumption is that the scraper is installed in a region of $\pi<\phi_{sc}\leqq 3\pi/2$ in the rotating direction from the cylinder top while completely scraping off the condensate film.

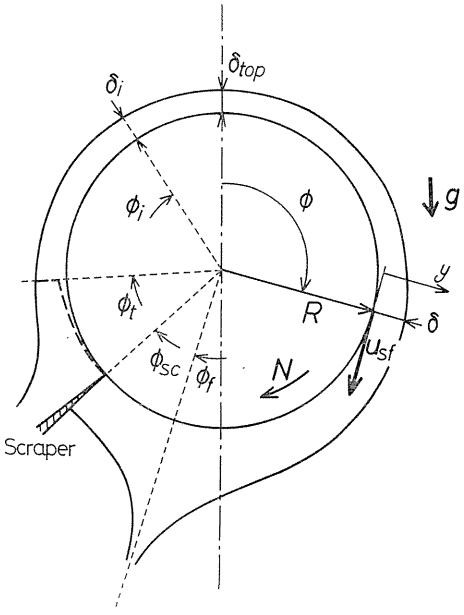

Fig. 2. 1 Analytical model.

2. 1. Fundamental equations

Referring to the method of Singer, et al.[9], fundamental equations are derived. Assumptions include that the effects of inertia force and vapor friction are neglected for the condensate film and that the sensible-heat transport by convection is also neglected. Then, velocity u and temperature T become as follows:

$$u=\frac{\rho_L-\rho_V}{2\rho_L\nu_L}g\sin\phi\delta^2\left[2\frac{y}{\delta}-\left(\frac{y}{\delta}\right)^2\right]+u_{sf} \tag{1}$$

$$T=T_s+(T_s-T_w)\left(\frac{y}{\delta}-1\right) \tag{2}$$

where ϕ is an angle from the cylinder top in the rotating direction, y is the radial distance outward from the cylinder surface, δ is the thickness of condensate film, $u_{sf}=2\pi RN$ is the peripheral speed on the outer surface of the cylinder, T_s and T_w are the temperatures of saturated vapor and the wall surface of the cylinder. On the other hand, the equation of heat balance is expressed as follows for the entire condensate film flowing in between positions $\phi=0$ to $\phi=\phi$.

$$\rho_L L\left[\left(\int_0^\delta u\,dy\right)_{\phi=\phi}-\left(\int_0^\delta u\,dy\right)_{\phi=0}\right]$$
$$=\lambda_L\int_0^\phi\left(\frac{\partial T}{\partial y}\right)_{y=0}Rd\phi \tag{3}$$

By substituting Eqs. (1) and (2) in Eq. (3), Eq. (3) is reduced dimensionless by differentiating with ϕ, as follows:

$$\frac{d\hat{\delta}}{d\phi}=\frac{1-\cos\phi\hat{\delta}^4}{3(\sin\phi\hat{\delta}^3+A^{1/2}\hat{\delta})} \tag{4}$$

where the unit of ϕ is radian, and dimensionless parameter A and dimensionless condensate film thickness $\hat{\delta}$ are given by the following equations.

$$A\equiv\frac{PrRe_R^2}{3Gr_RH}=\frac{4\pi^2}{3}\frac{Pr}{Gr_RH}\left(\frac{NR^2}{\nu_L}\right)^2$$

$$\hat{\delta}\equiv\left(\frac{Gr_RPr}{3H}\right)^{1/4}\frac{\delta}{R}$$

In these equations of defining A and $\hat{\delta}$, dimensionless numbers are defined as follows:

$$Gr_R\equiv\frac{R^3g(\rho_L-\rho_V)}{\rho_L\nu_L^2}$$

$$Pr\equiv\frac{c_{PL}\rho_L\nu_L}{\lambda_L}$$

$$H\equiv\frac{c_{PL}(T_s-T_w)}{L}$$

$$Re_R\equiv\frac{u_{sf}R}{\nu_L}$$

The square root of dimensionless parameter A is equivalent to the product of the rotation speed and the time to achieve steady state as introduced in the previous chapter for the vertical cylinder; only different is the characteristic length.

2. 2. Incidental conditions

Equation (4) shall be solved over the entire surface of the cylinder under suitable initial conditions. However, the following incidental conditions should be considered.

(i) Conditions for finiteness of the condensate film thickness at an angular position upper than the cylinder axis

When dimensionless parameter A is small, there is a value of ϕ that the denominator of the right side of Eq. (4) becomes 0, within a range $-\pi/2<\phi<\pi/2$. To have finite condensate film thickness, the numerator should simultaneously be 0. Namely, the following equation is established.

$$\left.\begin{aligned} &1-\cos\phi\hat{\delta}^4=0 \\ &3(\sin\phi\hat{\delta}^2+A^{1/2})=0 \end{aligned}\right\} \tag{5}$$

Putting these solutions ϕ_i and $\hat{\delta}_i$, the following equation is obtained.

$$\left.\begin{aligned} &\phi_i=-\cos^{-1}\left[-\frac{A}{2}+\left\{\left(\frac{A}{2}\right)^2+1\right\}^{1/2}\right] \\ &\hat{\delta}_i=(\cos\phi_i)^{-1/4} \end{aligned}\right\} \tag{6}$$

Here ϕ_i and $\hat{\delta}_i$ are the initial condition of Eq. (4) with a small A. From ϕ_i, solutions can be derived in positive and negative directions of ϕ.

(ii) Condition at the position of scraper

Flow rate per unit width $\dot{V}_{sc}$ at the position of scraper ϕ_{sc} is given by Eq. (7) from Eq. (1).

$$\frac{\dot{V}_{sc}}{Ru_{sf}}=\left\{\frac{Gr_R}{3Re_R}\sin\phi_{sc}\left(\frac{\delta_{sc}}{R}\right)^2+1\right\}\left(\frac{\delta_{sc}}{R}\right) \tag{7}$$

The lower surface of the scraper is against the rotating direction of the cylinder, at which there is a flow toward the scraper. However, the flow from the upper side of the cylinder is blocked by the scraper. Therefore, $\dot{V}_{sc}\geqq 0$ holds valid. In the opposite i.e. upper side, $\dot{V}_{sc}\leqq 0$ is true. If $\dot{V}_{sc}\neq 0$ in both sides, condensate liquid is separated from the cylinder surface at the scraper. In other words, this denotes the final position of the condensate film. On the other hand, when $\dot{V}_{sc}=0$, the following Eq. (8) is obtained from Eq. (7).

$$\left.\begin{aligned} &\frac{\delta_{sc}}{R}=0 \\ &\frac{\delta_{sc}}{R}=\left(-\frac{Gr_R}{3Re_R}\sin\phi_{sc}\right)^{-1/2} \end{aligned}\right\} \tag{8}$$

In the lower surface of the scraper, condensate film will have a finite thickness, that is, the solution becomes the second value of Eq. (8). In the upper side, on the other hand, the condensate film will have infinitesimal thickness, that is, the solution becomes the first value of Eq. (8). As described above, the case of $\dot{V}_{sc}=0$ results in determining the condensate film thickness, i.e. providing the initial condition of Eq. (4). Consequently, in this case, the following condition of (iii) is required.

(iii) Conditions for conformity or selection of solutions under the two initial conditions

This is a condition due to having a solution for each of the two initial conditions. The following three cases can be assumed; ① solutions from ϕ_i in the positive and

the negative directions without scraper, ② a solution from the scraper in negative direction and a solution from ϕ_i in positive direction, and ③ a solution from the scraper in positive direction and the other solution from ϕ_i in negative direction. In the cases of ① and ②, the conditions give the falling position of condensate film ϕ_f in the lower surface of the cylinder; as far as two solutions exist simultaneously, it is assumed that the solution of larger total momentum of condensate film should be prevailing, then a falling position is allocated to the position where the δ of that solution becomes infinite. In the case of ③, it is assumed that solution transition occurs at a position ϕ_t where the total flow rate of condensate film for each solution becomes the same.

By combining the incidental conditions above, the states of condensate film can be classified as shown in Table 1; a case without scraper and the *A*-1, *A*-2, *A*-*B*, *B*-1 and *B*-2 types for cases with scraper. Referring to the table, the ○ marks in columns (i) and (iii) show the application of relating conditions. In column (ii), positive or zero and negative conditions of $\dot{V}_{sc}$ are denoted. Practical examples for these types will be described in more detail in the later.

Table 1 Combination of incidental conditions.

Type of Condensate State		without Scraper	with Scraper				
			A-1	A-2	A-B	B-1	B-2
(i)	(ϕ_i)	○	○	○	○	—	—
(ii)	V_{sc} (Upside)		< 0	< 0	= 0	= 0	= 0
	V_{sc} (Downside)		= 0	> 0	= 0	= 0	> 0
(iii)	① (ϕ_f)	○					
	② (ϕ_f)		○	—	○	○	—
	③ (ϕ_t)		—	—	○	—	—

2. 3. Method of analysis

2. 3. 1. Distribution of condensate film thickness

Equation (4) was numerically integrated using the initial conditions shown in the paragraph 2. 2, by the Adams method[17], thereby condensate film thickness δ was obtained. However, if the initial conditions were rigorously employed, there was a problem for numerical calculation. Therefore, the initial values for δ or ϕ were slightly adjusted by such amounts that no adverse influences would be created.

2. 3. 2. Nusselt number

Local heat transfer coefficient α_ϕ and local Nusselt number Nu_ϕ are defined as follows:

$$\alpha_\phi \equiv \frac{\lambda_L}{\delta}, \quad Nu_\phi \equiv \frac{\alpha_\phi R}{\lambda_L} = \frac{R}{\delta} \tag{9}$$

These values can be calculated using δ obtained in the previous paragraph. In addition, mean heat transfer coefficient α_m and mean Nusselt number Nu_m are defined as follows:

$$\alpha_m \equiv \frac{1}{2\pi}\int_0^{2\pi} \alpha_\phi d\phi, \quad Nu_m \equiv \frac{\alpha_m R}{\lambda_L} \tag{10}$$

Near the scraper, $\delta \fallingdotseq 0$ holds valid. Therefore, Nu_ϕ becomes very large and causes a large error when Nu_m is obtained by the numerical integral. Consequently, the analytical integral must be employed in this proximity, as follows: In Eq. (4), δ is assumed to be very small and the second term of the right side numerator is neglected. Then Eq. (11) is obtained.

$$\frac{d\hat{\delta}}{d\phi} = \frac{1}{3(\sin\phi\hat{\delta}^3 + A^{1/2}\hat{\delta})} \tag{11}$$

This equation can easily be solved analytically with $\sin\phi$ assumed constant. The actual method was that Nu_ϕ was obtained by Eq. (9), integration was performed in the vicinity of ϕ_{sc}, then the result was connected to the numerical integral.

In the numerical integral, the B-spline interpolation formula was used[18].

3. *Analyzed Results and Discussions*

Corresponding to the experiment in Chapter 3, an example of numerical calculations with refrigerant R-11 is shown with constant values at characteristic temperatures. Physical properties are used at 293.2 K and 303.2 K for liquid and vapor phases, respectively[13]. Also, the parameters used for presentation are temperature difference between saturated vapor and the heat transfer surface $\Delta T = T_s - T_w$(K) and rotation speed N (rpm) with constant value of the cylinder radius $R = 0.0375$ m.

3. 1. *Without scraper*

In this case, the incidental conditions of Table 1 beomes a combination of (i) and (iii) ①.

3. 1. 1. *Distribution of condensate film thickness*

As described in the paragraph 2. 3. 1, the initial value of δ was adjusted by

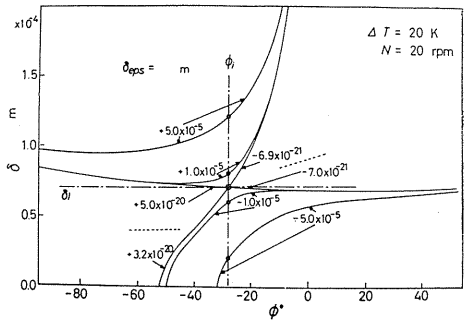

Fig. 2. 2 Effects of δ_{eps} on numerical solutions.

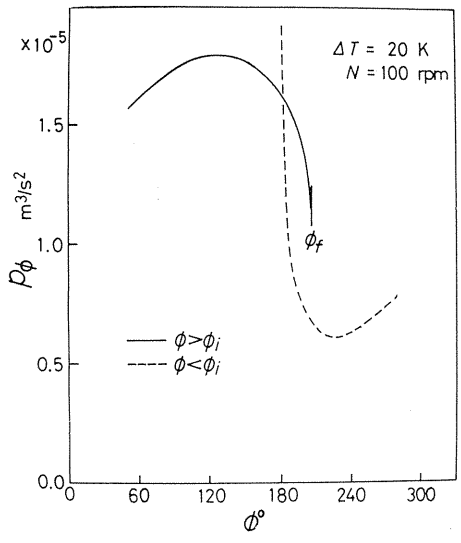

Fig. 2. 3 Total momentum of condensate film in the vicinity of ϕ_f.

very small amount δ_{eps} to apply the initial condition. An example of the difference of the numerical solution on this δ_{eps} is shown in Fig. 2. 2. Based on incidental condition (i), ϕ_i and δ_i can rigorously be calculated using Eq. (6). Referring to this δ_i, adjustment was applied within a range $\delta_{eps}=-5.0\times10^{-5}\sim+5.0\times10^{-5}$m. As a result, it is revealed that the solution of ϕ in the positive direction is valid in a range $\delta_{eps}<-7.0\times10^{-21}$m and the same in the negative direction is valid in a range $\delta_{eps}>+5.0\times10^{-20}$m.

Figure 2. 3 denotes an example with incidental condition (iii) ①. The total momentum of condensate film P_ϕ is defined by the following equation.

$$P_\phi=\int_0^\delta u|u|dy \tag{12}$$

In the close vicinity of ϕ_f in which there are two solutions, the P_ϕ of the solution in the positive direction of ϕ is larger, except at a position where δ becomes infinite. With other ΔT and N values, this tendency holds valid. Therefore, ϕ_f is to be set at the position where the solution in the positive direction of ϕ becomes infinite.

Figure 2. 4 denotes an example of condensate film thickness distribution. The condensate film thickness shows a bilateral asymmetry because of rotation, that is, $\phi>180°$ and the film becomes thicker in the left side. Especially, it is the thickest in vicinity of ϕ_f. Also, condensate film thickness becomes thicker with larger ΔT and N. Here ϕ_f is larger with smaller ΔT and larger N.

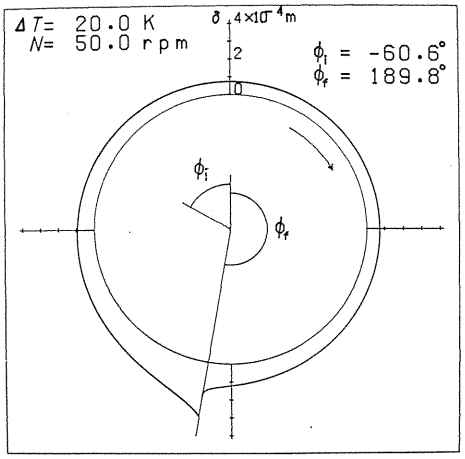

Fig. 2. 4 Distribution of condensate film thickness (Without scraper).

3. 1. 2. Heat transfer coefficient

The local heat transfer coefficient is

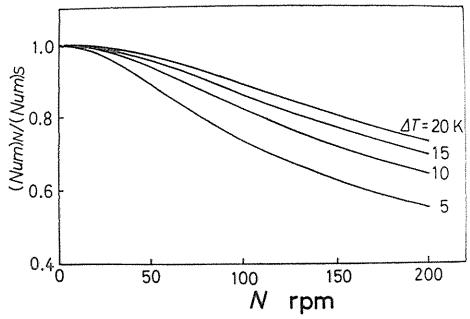

(a) Effect of N

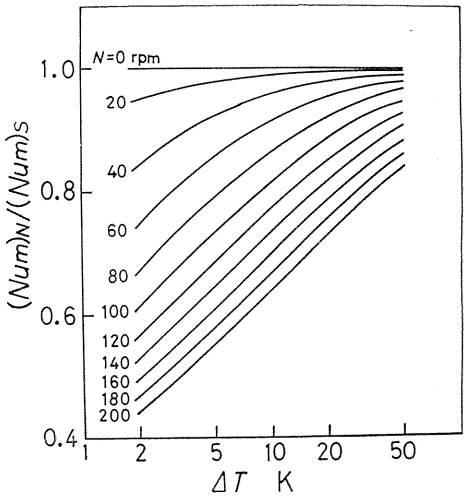

(b) Effect of ΔT

Fig. 2. 5 Mean Nusselt number ratio (Without scraper).

inversely proportional to δ, particularly, in the vicinity of ϕ_f, it is very small. Figures 2. 5 (a) and (b) denote the effect of N and ΔT on ratio $(Nu_m)_N/(Nu_m)_s$; the ratio concerns mean Nusselt numbers at $N=N$ and $N=0$. Ratio $(Nu_m)_N/(Nu_m)_s$ becomes smaller with larger N. This tendency is more significant with smaller ΔT. Also, the ratio becomes smaller with smaller ΔT. This tendency is more significant with larger N.

3. 2. With scraper

First, the case with scraper at $\phi_{sc}=-3\pi/4=-135°$ is described.

3. 2. 1. Distribution of condensate film thickness

States of condensate film can be classified to 4 types in the combination of the incidental conditions as shown in Table 1; as shown in Fig. 2. 6 with N and ΔT. Particularly, Figs. 2. 7 (a) and (b) denote the transition state of condensate film in the type A-B, where A and B denote solutions of condensate film thickness δ and total flow rate per unit width $\dot{V}_\phi$, for the negative and positive directions from the scraper position, respectively, starting from ϕ_i. Solutions B disappear with certain value of ϕ where $d\delta/d\phi$ is infinitive. Therefore, it would be most valid to assume that condensate film thickness be in transition at a point where $\dot{V}_\phi$ of A and B agree together, i.e. at $\phi=\phi_t$. Figure 2. 8 shows the distributions of δ in close proximity of the boundary between types A-B and B-1, with parameter N. In $N\leqq 48.7$rpm, $d\delta/d\phi$ becomes infinity but, in $N\geqq 48.8$ rpm, $d\delta/d\phi$ remains finite. Therefore, the latter

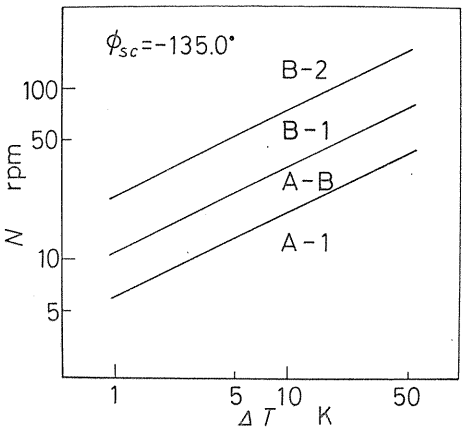

Fig. 2. 6 Classification of condensate film states.

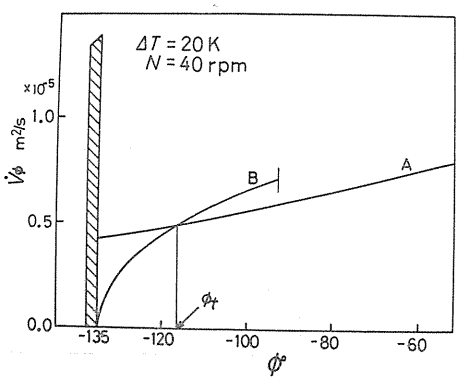

(a) Distribution of total flow rate of condensate film.

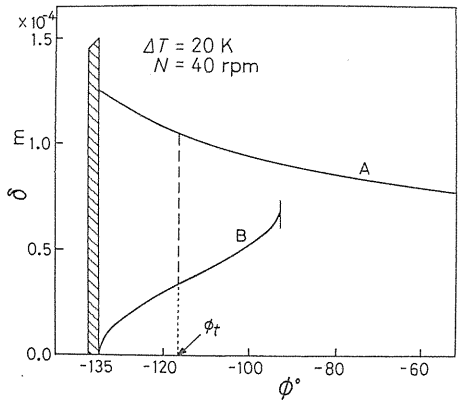

(b) Distribution of condensate film thickness.

Fig. 2. 7 Transition state of condensate film in the type A-B.

solution can be obtained to position $\phi=\phi_f$ without disappearance on the way.

The condensate film thickness distribution for each type is shown in Figs. 2. 9(a), (b), (c) and (d).

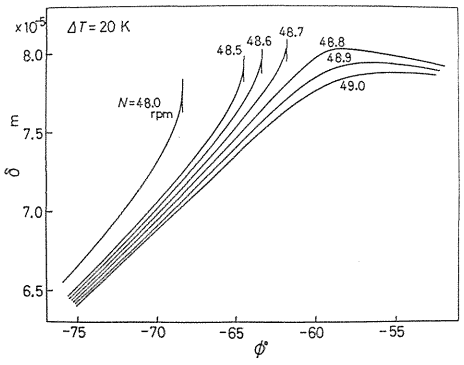

Fig. 2. 8 Distributions of condensate film thickness in the vicinity of the boundary between types A-B and B-1.

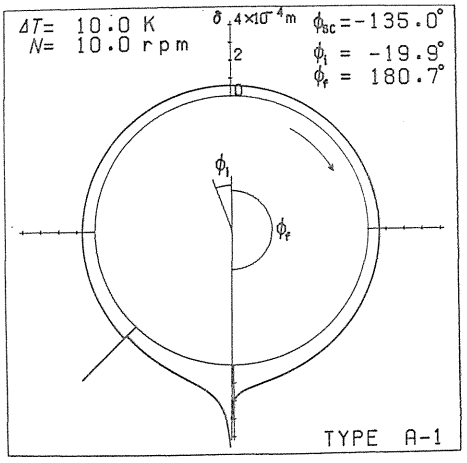

(a) Type A-1

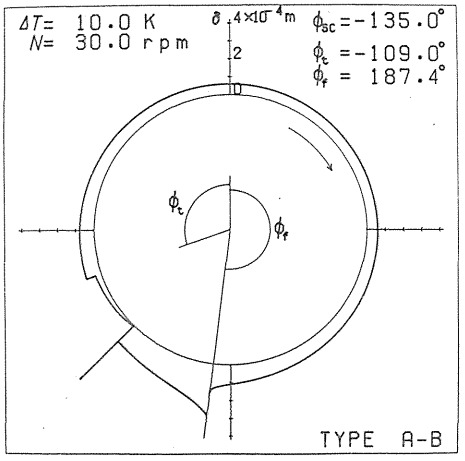

(b) Type A-B

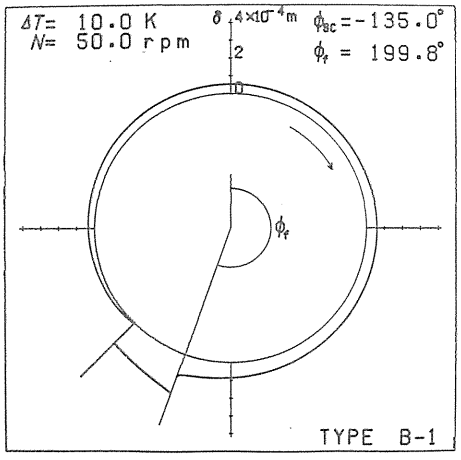

(c) Type B-1

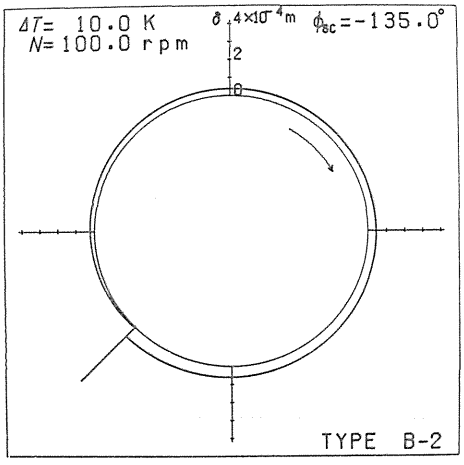

(d) Type B-2

Fig. 2. 9 Distributions of condensate film thickness (With scraper, $\phi_{sc}=-135°$).

3. 2. 2. *Heat transfer coefficient*

Figure 2. 10 shows a typical example of local heat transfer coefficient distribution, corresponding to Fig. 2. 9(b). Here α_ϕ becomes larger in the upper surface of the scraper where condensate film thickness is thin. It is smaller in the lower surface and in close proximity of ϕ_f. The effects of N and ΔT on the ratio of Nusselt numbers $(Nu_m)_N/(Nu_m)_s$ are shown in Figs. 2. 11 (a) and (b) ; the ratio concerns the mean Nusselt numbers at $N=N$ and $N=0$ without scraper. The ratio is slightly larger than 1 at $N=0$ and, when N increases, it decreases up to a certain value of N. When the value is exceeded, the ratio steeply increases. The smaller the ΔT, the larger the rate results. Also, with larger ΔT, the ratio decreases. In the figure, the types of

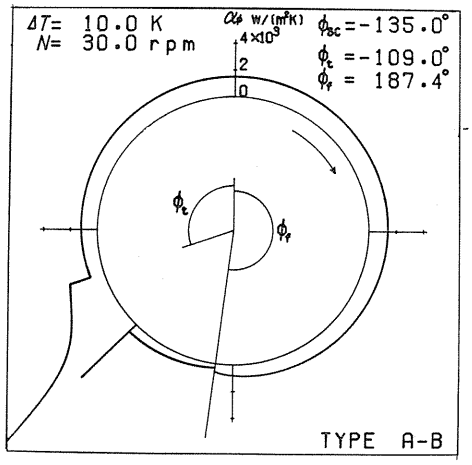

Fig. 2. 10 Distribution of local heat transfer coefficient (With scraper, $\phi_{sc}=-135°$).

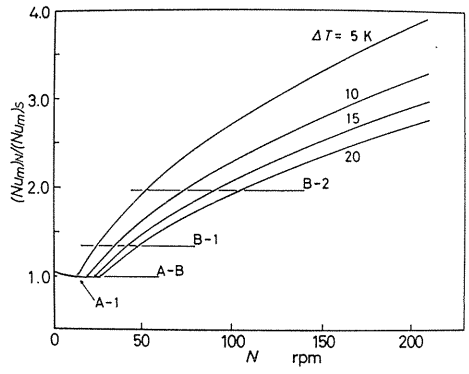

(a) Effect of N

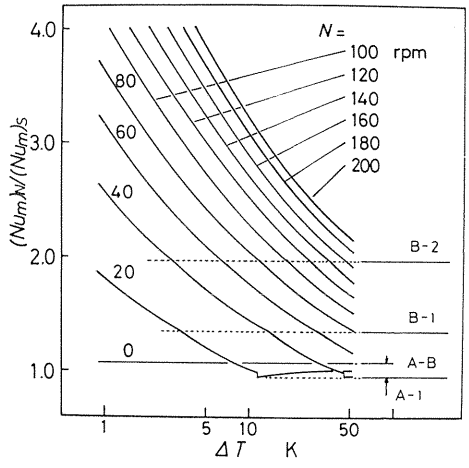

(b) Effect of ΔT

Fig. 2. 11 Mean Nusselt number ratio (With scraper, $\phi_{sc}=-135°$).

condensate state is described respectively. In the type A-1, substantially no effect is observed to augment heat transfer with a scraper. Therefore, it is understood that the rotation speed must be raised to create type A-B.

3. 2. 3. *Examination for position of scraper*

The description above relates to the case of $\phi_{sc}=-135°$. In this paragraph, the cases of $\phi_{sc}=-90°$ and $-179.5°(=-180°)$ are examined for comparison to study the effect of scraper installation position. The type of condensate state at $\phi_{sc}=-90°$ is similar to that at $\phi_{sc}=-135°$; however the region for type B-1 becomes wider in the former. In the case of $\phi_{sc}=-179.5°$; type A-2 appears and type B-1

disappears; the former type is not present at $\phi_{sc}=-135°$ and, in this type, the solutions in the positive direction from ϕ_i reach to the installation position of the scraper.

The effect of ϕ_{sc} on the heat transfer coefficient is shown in Fig. 2. 12. The value of α_m does not change so much depending on ϕ_{sc}, however, peaks appear at $\phi_{sc}=-90°$ and $-179.5°$ at smaller and larger N, respectively. When N further increases, the effect of the gravity becomes smaller, where the value α_m for each ϕ_{sc} agrees with each other.

For cases of other values of ϕ_{sc}, the same analysis can be performed.

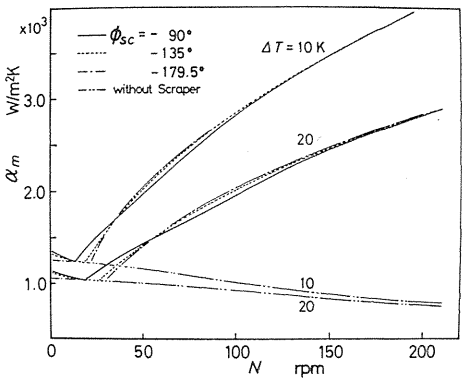

Fig. 2. 12 Effects of ϕ_{sc} on the heat transfer coefficient.

3. 3. *Dimensionless presentation*

In the paragraphs of 3. 1 and 3. 2, numerical examples are shown with the R-11 and parameters N and ΔT. In the present section, however, the relations are rearranged with dimensionless presentation; Figs. 2. 13(a), (b) and (c) denote for $\phi_{sc}=-3\pi/4$, $-\pi/2$ and $-\pi$(more precisely, $-179.5\pi/180$). Figure 2. 13(a) also

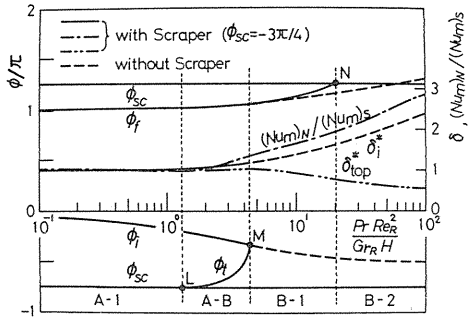

(a) $\phi_{sc}=-3\pi/4$

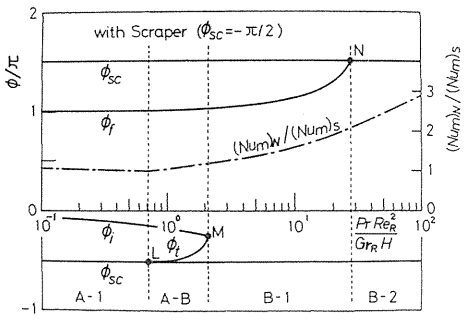

(b) $\phi_{sc}=-\pi/2$

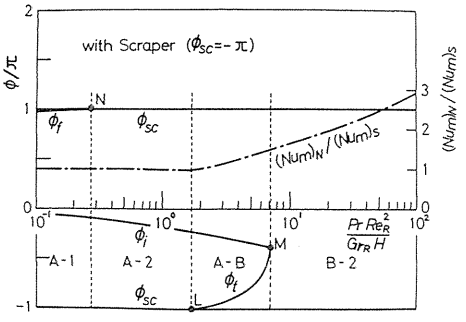

(c) $\phi_{sc}=-\pi$

Fig. 2. 13 Arrangement with dimensionless presentation.

shows a case without scraper in broken line. The abscissa represents dimensionless parameter $PrRe_R^2/Gr_RH$, while denoting the interrelationship between ϕ_i, ϕ_f, ϕ_t and ϕ_{sc}. The figure also shows the changes of δ_i^*, δ_{top}^* and $(Nu_m)_N/(Nu_m)_s$, where δ_i^* and δ_{top}^*, as shown only in Fig. 2. 13(a), relate to the values of dimensionless δ_i and δ at the top of the cylinder in non-rotation. Symbols L, M, and N represent three positions, i.e. the first position at which ϕ_t appears from ϕ_{sc}, the second position where ϕ_i agrees with ϕ_t and the solution from ϕ_i is no longer needed, and the third position in which ϕ_f and ϕ_{sc} agree together while ϕ_f disappears. These three positions represent the transition points between each condensate state type.

4. Conclusions

A new method was proposed to augment heat transfer in condensation; a horizontal cylinder was rotated and the condensate film was scraped off from the outer surface. According to a theoretical analysis, the following conclusions were obtained.

(1) The ordinary differential equations for the condensation on the outer surface of a horizontal cylinder have been derived with a variable of condensate film thickness. These equations have been solved by adding several incidental conditions that may physically be valid and numerically integrating. Using these solutions, the mean Nusselt numbers are obtained and the effect of scraping is quantitatively expressed by the mean Nusselt number ratio.

(2) The condensate state can be classified to various types depending on the combination of the incidental conditions. These types are shown.

(3) Without a scraper, the mean Nusselt number ratio becomes smaller when the rotation speed N is larger and temperature difference between saturated vapor and the condenser surface ΔT is smaller.

(4) With a scraper, the mean Nusselt number ratio steeply increases beyond the certain value of N. The smaller the ΔT, the larger the ratio results.

(5) Suitable installation positions of the scraper ϕ_{sc} are $\phi_{sc}=-90°$ at low rotation speed and $\phi_{sc}=-179.5°$ at high rotation speed. At more high rotation speed, this difference becomes smaller.

(6) The calculated results are rearranged with dimensionless presentation; it is expressed that all data for each ϕ_{sc} are governed by dimensionless parameter $PrRe_R^2/Gr_RH$.

Chapter 3. Experiment of Condensation on Outer Surface of Vertical and Horizontal Cylinder

1. Introduction

The rotating condenser has been reported by many researchers so far, including Nicol, et al.[8], Singer, et al.[9] for the vertical and horizontal cylinders, and many others[7] for different types. In either case, however, it is pointed out that the rotation speed should be high because the heat transfer efficiency is not substantially augmented at low speed range in each type. The authors' research is not intended to improve the heat transfer effect at high rotation speed, because a large amount of driving force would be required. Instead, our interest is mainly focused on rather

lower speed that would be more beneficial in view of energy conservation and low-cost equipment.

In these points of view, the authors have proposed a new equipment, the rotating condenser with a scraper to augment heat transfer coefficient in condensing phase; a cylindrical condenser is rotated around the axis, then a scraper is closely attached onto its outer surface while being positioned parallel to the rotating axis, thereby the scraper scrapes off the condensate film which otherwise will work as a heat resistance. In Chapter 1 and Chapter 2, the effect of scraping and the condensate film conditions was analyzed with the vertical and horizontal scraper cylinders. In the present chapter, an experiment to prove this analysis is described; the scraper effect is presented as a function of the heat transfer coefficient and the mean Nusselt number. Also, the influence of rotation speed and temperature difference is clearly denoted. Thus, practical problems are studied in comparison with the theoretical results. In addition, other technical assessments are also described including how to seal the rotation axis, suitable material for the scraper, installation method, etc.

2. Experlimental Apparatus and Procedures

Figure 3. 1 shows an outline of the experimental apparatus. This relates to the horizontal cylinder type. The vertical one is substantially the same, so that the following description deals only with the horizontal type. Referring to Fig. 3. 1, the solid lines including arrows show the refrigerant circuit. The total refrigerant circuit was evacuated about 1 hour, thereby non-condensable gas was almost completely purged. Then, evaporator ② was activated to generate saturated vapor of refrigerant *R*-11. Then vapor speed is sufficiently retarded in mixing chamber ⑥, and enter chamber ⑧. Most of the refrigerant vapor is condensed on a cylindrical condenser in the chamber, then the condensate passes condensate meter ⑨ and returns to evaporator ②, thereby natural circulation is completed. In the case of the vertical cylinder, liquid refrigerant flow was controlled using a gear pump to charge forcefully in the evaporator; namely a forced circulation system was employed. In the cooling water circuit as shown by the arrow of broken lines, water is cooled at a specified inlet temperature by refrigerator ⑬ and flow rate is set by means of control valve ⑮ and flow meter ⑯. Then, the water passes inside the cylindrical condenser and returns to the refrigerator.

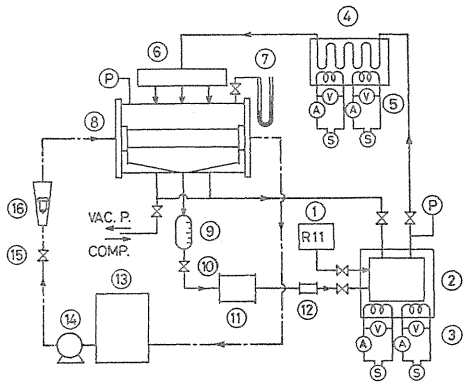

Fig. 3. 1 Schematic diagram of experimental apparatus.

Figures 3. 2 (a) and (b) detail the vertical cylinder type condenser. The equipment unit in (a) consists of a box type chamber made of stainless steel and a vertical, cylindrical copper condenser of 101 mm OD, 705 mm height, and 0. 2237 m^2 heat transfer surface area. The shaft sealing of the rotary part is ensured by the double array mechanical seals on both ends. Cooling water flows from the bottom of the cylinder to the upper (B to B′). Inlet and outlet temperatures were measured

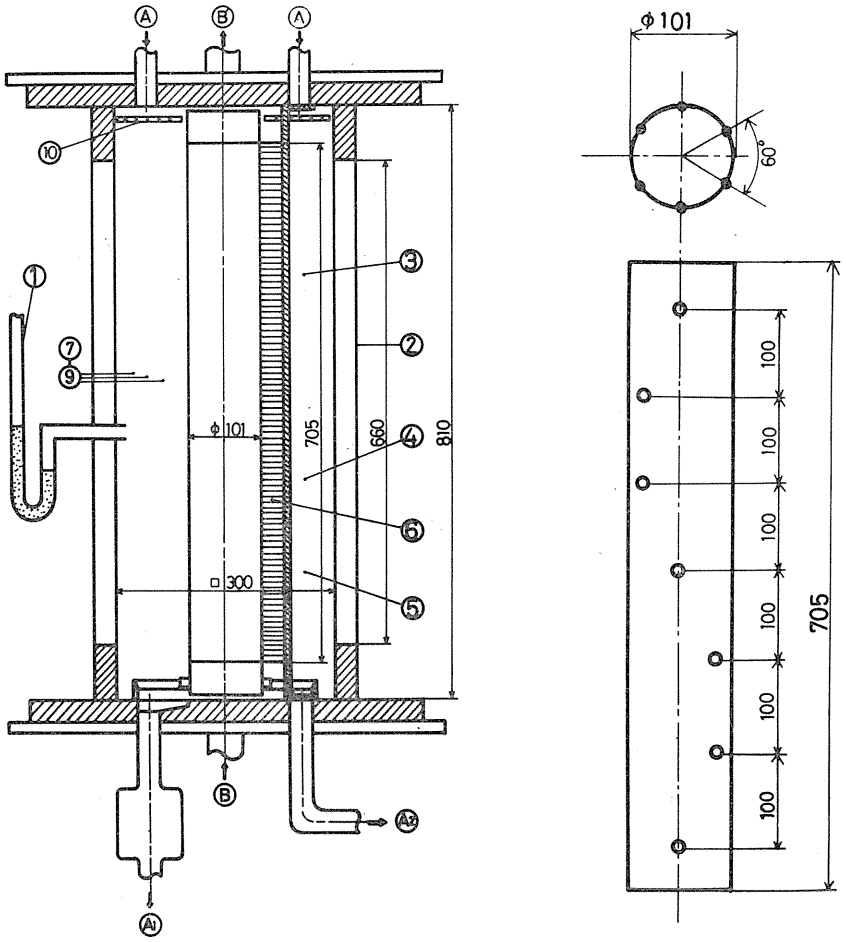

(a) Equipment unit. (b) Heat transfer surface.

Fig. 3. 2 Details of test section (Vertical cylinder).

using the 0.3 mm ϕ copper constantan (C-C) thermocouples. Vapor temperatures in the chamber were measured with the thermocouples above installed in 3 positions each in vertical and horizontal directions in the chamber, as shown in the figure. Measurement of the temperature on the heat transfer surface is outlined in Fig. 3. 2 (b); the 0.3 mm ϕ C-C themocouples were placed at 7 positions in a spiral formation in the axial direction, then their outputs were continuously recorded in a multi-pen recorder via the slipring unit. Condensate liquid film was scraped off using Teflon scraper ⑥ positioned parallel to the cylinder axis and in close contact with the surface.

Figures 3. 3 (a) and (b) detail the horizontal, cylindrical condenser. The unit of (a) consists of a copper-plated cylindrical chamber and a horizontal, cylindrical copper condenser of 75 mm OD, 600 mm length, and 0.1414m^2 heat transfer area. The rotary unit is sealed by the same method as in the vertical cylinder. Vapor temperatures in the chamber were measured using the thermocouples installed at 3

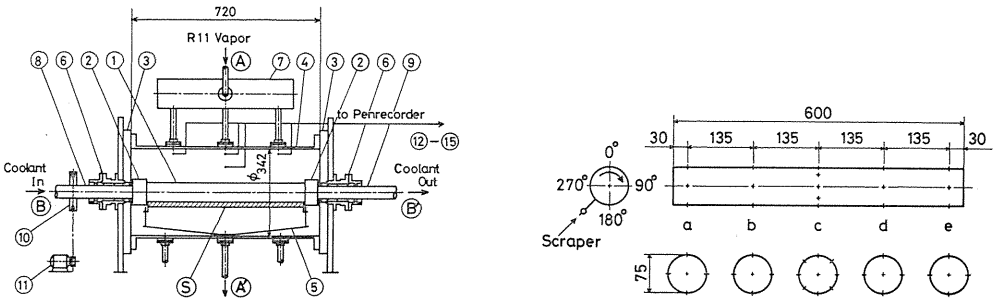

(a) Equipment unit. (b) Heat transfer surface.

Fig. 3. 3 Details of test section (Horizontal cylinder).

positions in the vapor inlet and at a position in the chamber center. To scrape off condensate film, a Teflon rubber scraper (600 mm length, 27 mm width, 1. 0 mm thickness) Ⓢ was positioned parallel to the cylindrical axis and in close contact with the surface. Its installation position for the experiment was as shown in Fig. 3. 3 (b); an angle $\phi_{sc}=225°$ was taken from the top in the rotating direction. Also, temperatures of the heat transfer surface were measured using the 0. 3 mm ϕ C-C thermocouples installed in 5 positions in the axial direction and 4 positions in circumferential direction (8 points at the center), namely in 24 positions in a total. The output was read using a recorder via the slip-ring unit. This slip-ring unit was comprised of a copper and a constantan ring to prevent contact error of the thermocouple.

The following procedures of the experiment were commonly employed for both vertical and horizontal cylinders.

Saturated vapor temperature T_s was set referring to the respective saturation pressure P_s. Here P_s was measured using a mercury manometer in high precision. Rate of condensation $\dot{m}$ was calculated by $\dot{m}=\rho_L V/t$ after measuring time t of filling volume V of the measuring cylinder. Here ρ_L is condensate liquid density. To vary temperature difference ΔT between T_s and heat transfer surface temperature T_{wm}, the experiment was performed while changing T_s, cooling water inlet temperature T_b, and flow rate Q_b. A variable speed motor was employed to rotate the setup, with a rotation accuracy of less than $\pm 2\%$. Mean heat transfer coefficient α_m was calculated as follows : measured temperatures of 7 points for the vertical cylinder or 24 points for the horizontal cylinder were averaged for mean temperature T_{wm} representing the total heat transfer surface as a characteristic temperature. Mean heat transfer coefficient α_m was calculated by the following equation.

$$\alpha_m=(Q/A)/(T_s-T_{wm})$$

Neglecting the quantity of heat used for subcooling in condensate liquid, $Q=\dot{m}L$ is obtained, where L is the latent heat for condensation.

3. Experimental Results and Discussions

3. 1. Condensation on the outer surface of vertical cylinder

3. 1. 1. Non rotation

In this case, the normal condensation of gravitational free convection heat

transfer occurs. The relations between Nu_m and Ga_lPr/H obtained in the experiment is shown in Fig. 3. 4. The bold solid line denotes the theoretical value of Nusselt[19]. The experimental values are slightly smaller than the theoretical values. The difference may come from the negligence of condensate subcooling, accuracy of physical properties and surface temperatures, accuracy of theoretical value itself, etc.

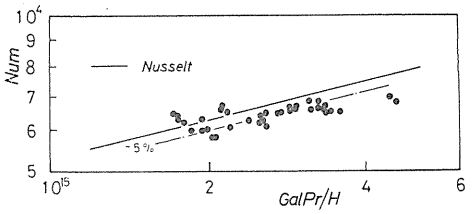

Fig. 3. 4 Relations between Nu_m and Ga_lPr/H (Vertical cylinder, non rotation).

3. 1. 2. Without scraper in rotation

Figure 3. 5 shows an example of the relations between mean Nusselt number ratio $(Nu_m)_N/(Nu_m)_{N=0}$ and rotation speed N. Referring to the analysis in Chapter 1, this ratio should constantly be 1 because of the assumption in use. Although the experimental values were considerably scattered, the ratios were about 0. 9, generally smaller than 1. As obvious from these facts, the condensate film will not be splashed away by the centrifugal force at a maximum of about 120 rpm as in this experiment. In addition, the shear force with static vapor in the liquid-vapor interface acts only in the circumferential direction. Therefore, it is obvious that the shear force is not effective to expedite the flow down speed of condensate film or to disturb it.

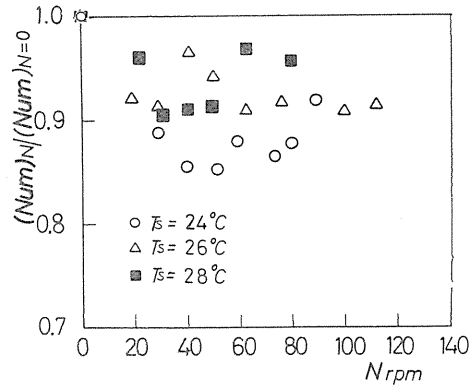

Fig. 3. 5 Relations between $(Nu_m)_N/(Nu_m)_{N=0}$ and N (Vertical cylinder, without scraper).

3. 1. 3. With scraper in rotation

Figure 3. 6 shows the relations of heat transfer coefficient α_m and ΔT with a parameter of N. The solid lines and broken lines herein relate to a case in the analysis of Chapter 1, with the remaining thicknesses after scraping $\delta_0=0.0$ and 0. 03 mm. The experimental value becomes fairly larger when N is larger, than with $N=0$; with $N=80$ rpm, the value becomes about 2 times. This is because, when N is larger, the time from one scraping to the next is resulted shorter, so that the condensate film thickness becomes thinner. Also, when comparing to the theoretical value, the experimental value is closer to the calculation with $\delta_0=0.03$ mm. It would imply that similar thickness of unscraped film might have remained in the experiment. Figure 3. 7 denotes the height distribution of the dimensionless heat transfer surface temperature with a parameter of N. The larger the N, the temperature of heat transfer surface becomes generally higher. This would be because, with larger N, the coefficient of condensation heat transfer increases as described above. In general, the coefficient of heat transfer is larger in upper heat transfer surface. Therefore, the temperature of heat transfer surfa ce would be higher in the upper part. With small N, the experimental value agrees with this

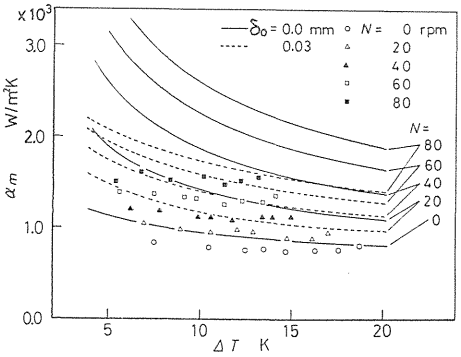

Fig. 3. 6 Relations between α_m and ΔT (Vertical cylinder, with scraper).

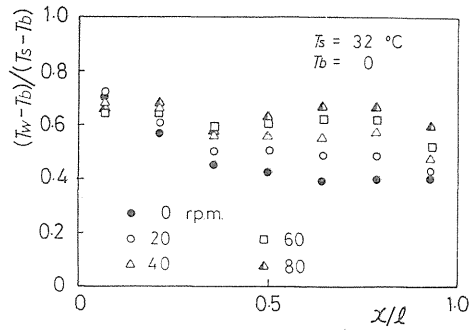

Fig. 3. 7 Distributions of $(T_w-T_b)/(T_s-T_b)$ (Vertical cylinder, with scraper).

hypothesis. However, with larger N, the value at $x/l=0.6\sim 0.8$ becomes higher. This is not explained only with the result of the present experiment, however, the cooling-side coefficient inside the rotary cylinder may have relations.

3. 2. Condensation on the outer surface of horizontal cylinder

3. 2. 1. Non rotation

Figure 3. 8 shows the relations between Nu_m and Ga_dPr/H obtained in the experiment, like in Fig. 3. 4. The bold solid line denotes the theoretical value of Nusselt[20]. In general, the experimental values are lower than the theoretical values. The cause would be the same as in the discussion on Fig. 3. 4.

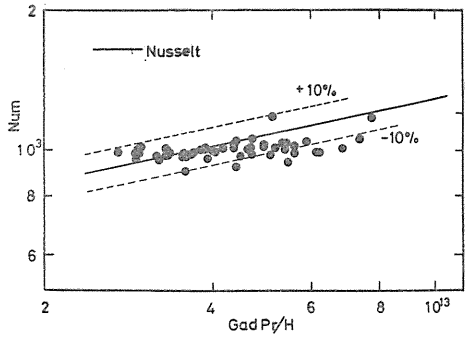

Fig. 3. 8 Relations between Nu_m and Ga_dPr/H (Horizontal cylinder, non rotation).

3. 2. 2. Without scraper in rotation

Figures 3. 9 (a) and (b) show the influence of N and ΔT on the mean Nusselt number ratio $(Nu_m)_N/(Nu_m)_s$, where the solid lines relates to the result of an analysis in Chapter 2. The larger the N and smaller the ΔT are, the smaller this ratio results. Compared to the analytical value, the experimental values are generally smaller, however, the latter show the same tendency as the theory, except in lower rotating region. That is, the values become smaller with larger N and smaller ΔT. Particularly at $N=120$ rpm, the ratio drops by a maximum of about 30 %. Without the scraper, heat transfer cannot be augmented, like in the vertical cylinder. Instead, condensate film tends to be stagnated in the rising side of a rotating cylinder, resulting in thicker condensate film. As a result, heat transfer coefficient was rather degraded. Figures 3. 10 (a) and (b) show the examples of condensate film photos; $\Delta T\fallingdotseq 17$K, $N=40$ and 120 rpm. These photos show a view

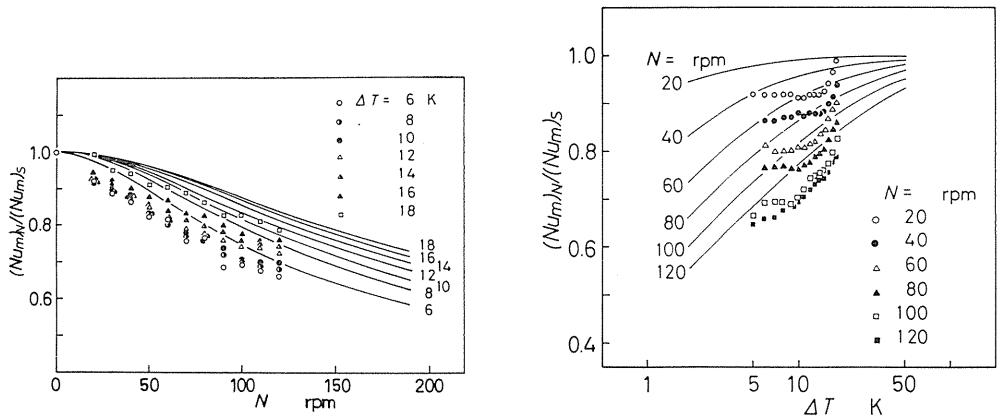

(a) Effects of N (b) Effects of ΔT

Fig. 3. 9 Effects of N and ΔT on $(Nu_m)_N/(Nu_m)_s$ (Horizontal cylinder, without scraper).

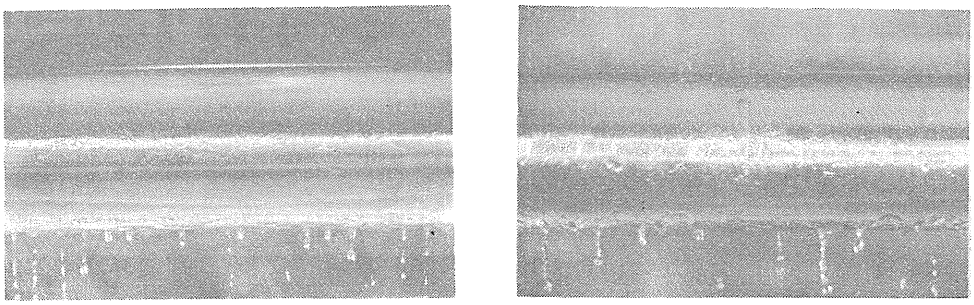

(a) N=40 rpm (b) N=120 rpm

Fig. 3. 10 Photos of condensate film (Horizontal cylinder, without scraper).

on the rising wall side of the cylinder from a point 270° in the rotating direction from the cylinder top. According to an analytical result, separating positions of condensate film are 188° and 214°; the angles become larger with larger rotation speed N. Also, the thickness of condensate liquid film results larger as the N is larger. This tendency can qualitatively be observed in the photos.

3. 2. 3. With scraper in rotation

Figure 3. 11 shows the relations between heat transfer coefficient α_m and ΔT, with a parameter of N. The smaller the ΔT and the larger the N, the α_m is larger, except in $\Delta T<6$K and $N\leqq 20$ rpm. Especially the heat transfer coefficient with $N=200$ rpm is about 2.5 as large as with $N=0$ rpm. These experimental results are compared with the analytical values in Chapter 2; these data were rearranged in terms of the mean Nusselt

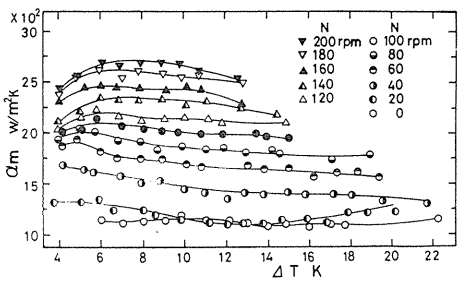

Fig. 3. 11 Relations between α_m and ΔT (Horizontal cylinder, with scraper).

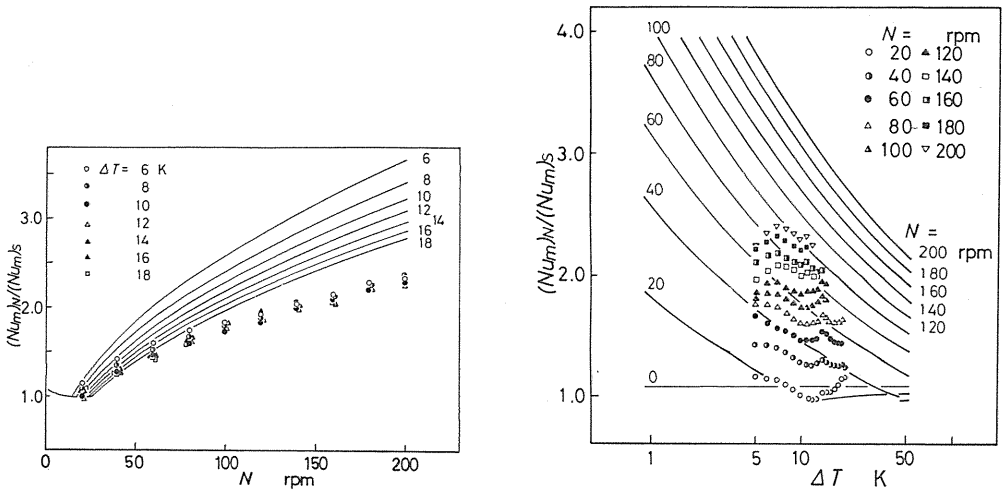

(a) Effects of N (b) Effects of ΔT

Fig. 3. 12 Effects of N and ΔT on $(Nu_m)_N/(Nu_m)_s$ (Horizontal cylinder, with scraper).

number ratio between each rotation speed N and $N=0$, i.e. $(Nu_m)_N/(Nu_m)_s$. Figures 3. 12 (a) and (b) show the influence of N and ΔT against this ratio; in which unscraped film thickness δ_0 is not taken into account, that is, the data relates to $\delta_0=$ 0. 0 mm. The experimental values are, compared with the analytical values, considerably smaller when N is larger, with a smaller fluctuation concerning ΔT. For the case of vertical cylinder, Fig. 3. 6 shows the influence of the unscraped film thickness. It can be assumed that the result of the horizontal cylinder might have caused by the similar effect of the unscraped film thickness.

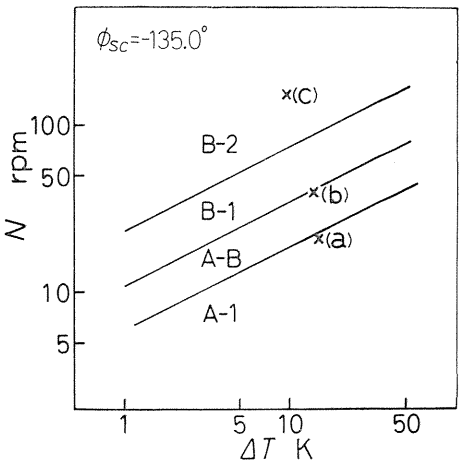

Fig. 3. 13 Classification of condensate film states (Horizontal cylinder, with scraper).

In the analysis of Chapter 2, the condensate film conditions were theoretically classified as shown in Fig. 3. 13; namely to types A-1, A-B, B-1 and B-2. The combinations of N and ΔT as shown in ×-marked (a), (b) and (c) are photographically shown in Fig. 3. 14 for respective condensate film states. The photographic viewing angle is the same as with Fig. 3. 10; that is, the photos show the rising side of the cylinder. The scraper is positioned at 225°(−135°) from the cylinder top. Figure 3. 14 (a) corresponds to type A-1, in which the condensate film is made fairly thick with some ripples and flows down from the upper side of the scraper. Figure. 3. 14 (b) represents type A-B; the condensate film is thin immediately on the scraper and steeply becomes thicker at a certain angle. Theoretical value of this angle is 286°(−74°). However, in the photo, the surface looks wavy

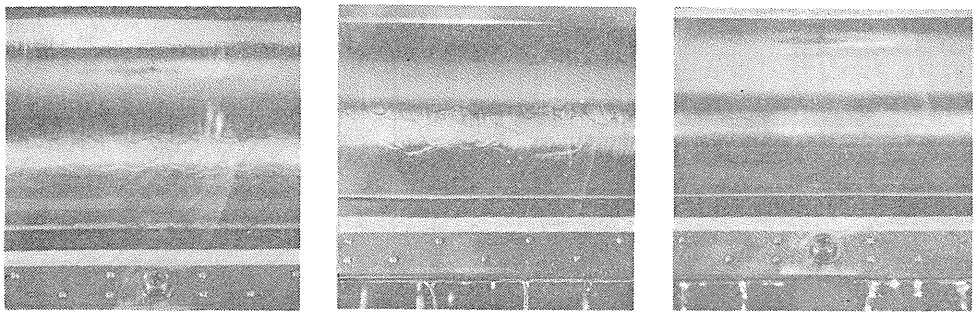

(a) $N=20$ rpm, $\Delta T=15.7$ K (b) $N=40$ rpm, $\Delta T=14.0$ K (c) $N=120$ rpm, $\Delta T=9.5$ K

Fig. 3. 14 Photos of condensate film (Horizontal cylinder, with scraper).

to horizontal direction while fluctuating timely, too. Figure 3. 14 (c) represents type B-2; the condensate film is generally thinner without any ripples. As described above, the experimental state of condensate is different from that of theoretical analysis, that is, not always two-dimensional or smooth and stationary. However, the data in average agree with the theoretical results.

4. Conclusions

According to the new method of augmenting heat transfer efficiency in condensation, the vertical and the horizontal cylinders were rotated and the condensate film was scraped off in the experiment using refrigerant *R*-11. The results were compared with the theoretical analysis, thereby the following conclusions were obtained.

(1) Without scraper in rotating vertical cylinder, experimental mean Nusselt number ratio $(Nu_m)_N/(Nu_m)_{N=0}$ was about 0. 9, while the theoretical value being 1. That is, there is no effect of augmenting heat transfer at low rotation speed.

With a scraper, effect of augmenting heat transfer was nearly doubled at $N=$ 80 rpm, compared with no rotation. The experimental value was close to the analytical value in consideration of unscraped thickness of condensate film.

(2) Without scraper in horizontal cylinder, the heat transfer coefficient drops at a maximum of about 30 % compared to non-rotation. This is because the condensate tends to stagnate on the heat transfer surface, while making condensate film thicker. These phenomena have visually been proved in a qualitative manner.

With a scraper, the heat transfer coefficient became about 2. 5 times as large as that in non-rotation, at $N=200$ rpm. This is rather small compared with the analytical result; it appears that the unscraped film thickness is affecting, in the same manner as conclusion (1).

Acknowledgement

The authors' thanks are due to the cooperations of the personnel in the laboratory of Prof. Izumi. The authors wish to thank the personnel of Computation Center of Nagoya University in the numerical calculations. This numerical calculations were carried out by the computer FACOM M-200. The authors are also grateful to

Mr. S. Kaga, Mr. A. Fujishiro and Mr. M. Hayakawa for their help in the experiments.

References

1) Fujii, T., Progress in Heat Transfer Engineering (in Japanese), Vol. 1 (1973), p. 8, Yokendo.
2) Hirasawa, S., et al., Trans. Japan Soc. Mech. Engrs. (in Japanese), Vol. 48, No. 427, B(1982-3), p. 527.
3) Hirasawa, S., et al., Trans. Japan Soc. Mech. Engrs. (in Japanese), Vol. 44, No. 382 (1978-6), p. 2041.
4) Yabe, A., et al., Trans. Japan Soc. Mech. Engrs. (in Japanese), Vol. 48, No. 435, B(1982-11), p. 2271.
5) Honda, H. and Mitsumori, K., Preprint of 19th National Heat Transfer Symposium of Japan (in Japanese), (1982-5), p. 349.
6) Sparrow, E. M. and Gregg, J. L., Trans. ASME, Sers. C, Vol. 81, No. 2 (1959-5), p. 113.
7) Sparrow, E. M. and Hartnett, J. P., Trans. ASME, Sers. C, Vol. 83, No. 1 (1961-2), p. 101.
8) Nicol, A. A. and Gacesa, M., Trans. ASME, Sers. C, Vol. 92, No. 1 (1970-2), p. 144.
9) for example, Singer, R. M. and Preckshot, G. W., Proc. Heat Transfer and Fluid Mech. Inst., No.14 (1963), p. 205, Stanford Univ. Press.
10) Shimada, R., et al., Trans. Japan Soc. Mech. Engrs. (in Japanese), Vol. 46, No. 407, B(1980-7), p. 1310.
11) Sparrow, E. M. and Siegel, R., Trans. ASME, Sers. E, Vol. 26. No. 1 (1959-3), p. 120.
12) Смирнов, В.И., Курс высщей математики, т. Ⅳ, Физматгиз, (1958～1960).
13) JAOR, Refrigeration (in Japanese), Vol. 52, No. 600 (1977-10), p. 3.
14) Hoyle, R. and Mathews, D. H., Int. J. Heat and Mass Transfer, Vol. 7 (1964), p. 1223.
15) Chandra, S., et al., Letters in Heat Mass Transfer, Vol. 3, No. 3 (1976), p. 239.
16) McElhiney, J. E. and Preckshot, G. W., Int. J. Heat and Mass Transfer, Vol. 20, No. 8 (1977-8), p. 847.
17) Fujitsu, FACOM FORTRAN SSL Ⅱ, Manual (in Japanese), (1980), p. 427, Fujitsu.
18) p. 142 of Reference (17).
19) Fujii, T., Progress in Heat Transfer Engineering (in Japanese), Vol. 1 (1973), p. 17, Yokendo.
20) p. 59 of Reference (19).